Journal of Sound and Vibration 463 (2019) 114950

Contents lists available at ScienceDirect

Journal of Sound and Vibration

journal homepage: www.elsevier.com/locate/jsvi

Aeroacoustics research in Europe: The CEAS-ASC report on 2018 highlights

Denis Gély [a], Gareth J. Bennett [b,*]

[a] DAAA, Aerodynamics, Aeroelasticity, Acoustics Department, ONERA - The French Aerospace Lab, BP 72 - 29 Avenue de la Division Leclerc, 92322, Châtillon, France

[b] Department of Mechanical and Manufacturing Engineering, School of Engineering, Trinity College Dublin, The University of Dublin, D02 PN40, Ireland

ARTICLE INFO

Article history:
Received 8 July 2019
Revised 4 September 2019
Accepted 9 September 2019
Available online 19 September 2019
Handling Editor: J. Astley

ABSTRACT

The Council of European Aerospace Societies (CEAS) Aeroacoustics Specialists Committee (ASC) supports and promotes the interests of the scientific and industrial aeroacoustics community on a European scale and European aeronautics activities internationally. In this context, "aeroacoustics" encompasses all aerospace acoustics and related areas. Each year the committee highlights some of the research and development projects in Europe.

This paper is a report on highlights of aeroacoustics research in Europe in 2018, compiled from information provided to the ASC of the CEAS. In addition, during 2018, a number of research programmes involving aeroacoustics were funded by the European Commission. Some of the highlights from these programmes are also summarised in this article, as well as highlights from other programmes funded by national programmes or by industry. Furthermore, a concise summary of the CEAS-ASC annual scientific workshop: "Future Aircraft Design and Noise Impact" held in the Netherlands Aerospace Centre (NLR) – Amsterdam in September 2018 is included in this report.

Enquiries concerning all contributions should be addressed to the authors who are given at the end of each subsection.

1. CEAS-ASC workshop

The 22nd CEAS-ASC Annual Scientific Workshop was held in NLR Amsterdam, on September 6–7, 2018. Its topic was "Future Aircraft Design and Noise Impact" and it was organized by Harry Brouwer of NLR and in co-operation with the EU project ANIMA (Aviation Noise Impact Management through Novel Approaches). The focus of the workshop was on the relationship between aircraft design and noise impact. Contributions were invited from both the domains of technology and impact assessment and thus the overarching objective of the workshop was to encourage discussion and cooperation between researchers in low noise technologies on one hand and on noise impact assessment and mitigation on the other.

Topics on which contributions were invited included: ∘ Aircraft overall noise ∘ Noise propagation ∘ Auralization ∘ Noise impact of new architectures ∘ Boundary layer ingestion ∘ Distributed propulsion ∘ Single event models ∘ Metrics ∘ From wind tunnel data to noise impact assessment ∘ Noise impact of drones ∘ Non-acoustical factors.

A total of 33 abstracts were received, 27 of which were accepted by the workshop scientific committee. In addition, 4 researchers accepted an invitation to present a keynote overview:

* Corresponding author.
E-mail address: gareth.bennett@tcd.ie (G.J. Bennett).

https://doi.org/10.1016/j.jsv.2019.114950
0022-460X/

- Lothar Bertsch, DLR: 10 years of joint research at DLR and TU Braunschweig toward low-noise aircraft design - what did we achieve?
- Russell Thomas, NASA: Realizing NASA's Vision for Low Noise Subsonic Transport Aircraft.
- Infrid Legriffon & Laurent Sanders, ONERA: Single Event Noise Prediction at ONERA - Case of aircraft powered by contra-rotating open rotors.

The workshop was well-attended with 56 participants from 13 European countries and the USA. The participation from the USA was somewhat larger than on previous occasions with 6 participants from NASA, FAA, and Pennsylvania State University. Proceedings can be found at https://www.nlr.org/ceas-asc-2018-workshop/.

2. Airframe noise

2.1. Numerical study of fan noise installation effects using the Immersed Boundary Method

For several years, ONERA has been developing an innovative two-step CFD/CAA workflow based on solid surfaces described by unstructured meshes immersed in volume Cartesian grids. This so-called Immersed Boundary Method (IBM) is particularly efficient to evaluate acoustic engine installation effects on novel aircraft architectures. The methodology consists in, first, computing the mean flow around the geometry of interest with the CFD solver FastS [1], then use the CAA solver sAbrinA.v0 [2] to compute the propagation of acoustic waves generated by any kind of noise source. Both solvers are used in Cartesian mode and have their IBM pre-process based on the Cassiopee package [1]. The method allows to drastically reduce the mesh design efforts as well as the computational costs for both CFD and CAA stages. First validations of the methodology with no mean flow confirmed its efficiency and reliability [3].

This methodology has been successfully applied to study the installation effects, on the fan/OGV interaction noise, of two different implementations OWN and UWN (Over- and Under-Wing-Nacelle) of classic turbofans on ONERA's NOVA aircraft, accounting for realistic non-uniform mean flows at $M = 0.25$ (i.e. take-off/landing flight conditions). Instantaneous pressure fluctuations computed by the sAbrinA.v0 solver are plotted in Fig. 1 for the two configurations. Multiple interference patterns, mainly due to reflection/scattering effects on the solid surfaces and refraction effects due to the mean flow gradients, are clearly noticeable. The comparison of noise maps on the ground (see Fig. 2) shows that the OWN configuration brings noise reduction

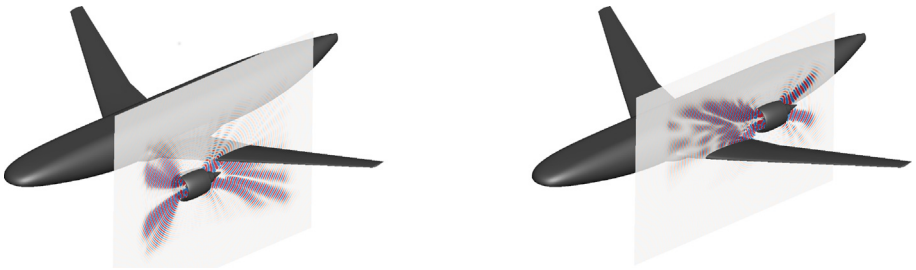

Fig. 1. Instantaneous pressure fluctuations with one-sided engine aircraft in the vertical nacelle mid-section plane: UWN configuration (a.); OWN configuration (b.).

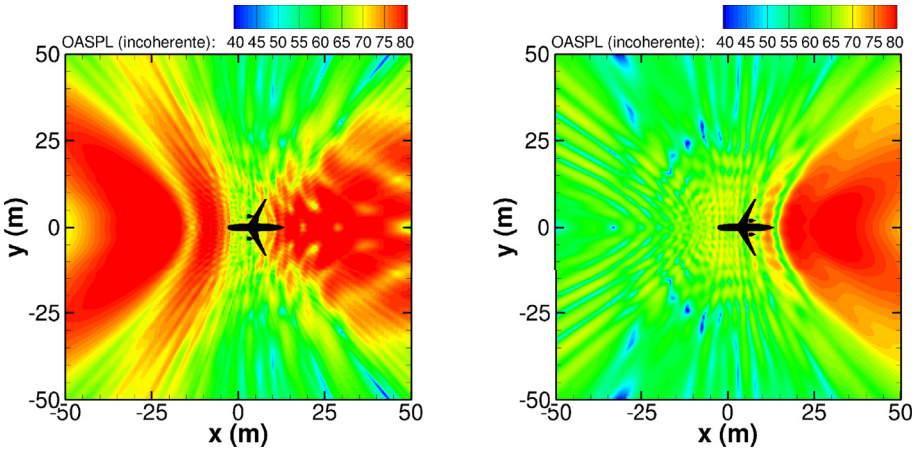

Fig. 2. Extrapolated acoustical pressure maps (in dB) with a two-sided engine aircraft: UWN configuration (left); OWN configuration (right).

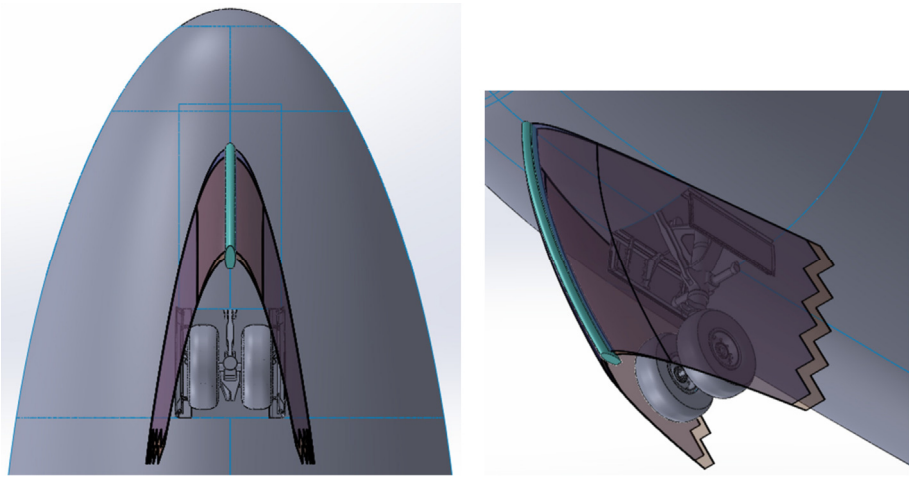

(a) Fuselage Mounted: Elevation (b) Fuselage Mounted: Isometric

Fig. 3. Dual-jet air curtain concept for shielding nose landing gear. Not to scale.

of more than 15 dB, especially in front of the aircraft as could be expected from this noise shielding effect.

These simulations demonstrate the capacities of the present numerical workflow. Parametric studies, dealing with acoustic efficiency for installation effects, are now affordable.

Written by Mathieu Lorteau: mathieu.lorteau@onera.fr*, Ludovic Wiart, Thomas Le Garrec, ONERA - The French Aerospace Lab, France*

2.2. The air curtain as a Fluidic Spoiler to reduce aerodynamic noise

The air curtain has been used in a number of diverse engineering applications, such as acting as smoke, heat or contamination barriers. In aeronautics, it was first proposed for use for landing-gear noise reduction by Wickerhoff and Sijpkes [4], after which Oerlemans and de Bruin [5] performed proof-of-concept research to validate it on a generic bluff body. In recent years, the planar jet as a means to reduce noise has been further investigated and advanced by Zhao et al. [6,7], in which tandem rods were examined as a simplified representation of aircraft landing gear. Subsequently, in order to minimise the additional noise source introduced by the air curtain itself, the "dual" air curtain has been developed and investigated, in which improved acoustic and energy efficiency have been achieved through the addition of a second upstream planar jet [8,9]. Initial research has been conducted into the development of the Fluidic Spoiler as a landing gear noise reduction technology beyond representative academic configurations, see Fig. 3. In addition to the acoustical studies, the fluid mechanics of dual planar jets in a cross flow, which have received little attention in the literature, have been extensively examined with PIV, hotwire and numerical analysis, and proper orthogonal decomposition has been performed in order to characterise the coherent structures of the flow field, particularly the large-scale vortices mainly occurring in the shear layers [10–12]. Further applications of the air curtain, also called: Fluidic Spoiler, have been studied such as the use of the air curtain to shield the aerodynamic noise of the pantograph of a high-speed train or to reduce cavity noise [13], see Fig. 4.

*Written by Gareth J. Bennett (*gareth.bennett@tcd.ie*) and Kun Zhao (*kzhao@tcd.ie*), Trinity College Dublin, the University of Dublin.*

2.3. Full scale nose landing gear analysis

Recently, research has been published based on the experimental results from the Clean Sky funded ALLEGRA "Advanced LowNoise Landing (Main and Nose) Gear for Regional Aircraft" project. This project was developed to assess low-noise technologies applied to a full-scale nose landing gear model and a half-scale main landing-gear model of a 90-seat configuration regional aircraft concept. With regard to the nose landing gear (NLG) campaign, one of the significant contributions of ALLEGRA is that a complete and highly detailed representation of the landing-gear components and associated structures such as the complete wheel bay cavity (wheel well), bay doors, nose fuselage and hydraulic dressings were included at full scale [14–16]. In 2018, results from a decomposition analysis was performed where LG components were removed one after the other in order to assess their individual contribution [17]. In addition, low noise treatments such as wheel hub caps, retractable fuselage fairings, perforated fairings and wire mesh were evaluated, see Fig. 5. Additional interesting findings such as the excitation and radiation of wheel well noise was assessed, in particular, the higher order modes of the large volume wheel well which can be excited within the velocity range of a landing aircraft [18]; modes that are usually ignored [19]. Also in 2018, windtunnel results were

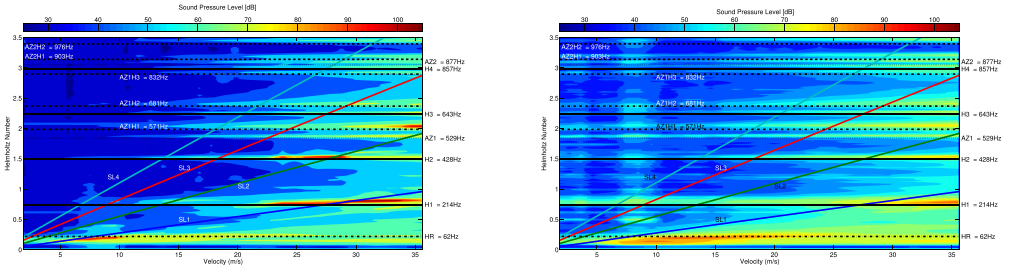

(a) Cavity resonance baseline.

(b) Fluidic spoiler applied upstream of cavity opening showing dramatic reduction in cavity pressure across all resonant modes.

Fig. 4. Sound pressure level [dB] inside a cylindrical cavity as a function of tunnel flow-speed. Superimposed on the plot are the theoretical shear layer modes (SL), the theoretical acoustic resonant modes, including azimuthal, (H1, AZ1…) and the Helmholtz resonance (HR).

(a) Without hub-caps applied

(b) With hub caps applied

Fig. 5. Hub-caps low noise technology applied to nose landing gear.

compared to flyover results of real aircraft of a similar size and design as well as to standard semi-empirical models. Particularly novel was the comparison to acoustic data extracted from CFD flow computations which was propagated to simulated microphone arrays and processed using several beamforming approaches [20]. Similar analyses were performed for the half-scale MLG which also was found to radiate noise from the wheel bay [21,22].

*Written by Gareth J. Bennett (*gareth.bennett@tcd.ie*) and John Kennedy (*kennedj@tcd.ie*), Trinity College Dublin, the University of Dublin. Ireland*

2.4. Numerical analysis of the impact of variable porosity on trailing-edge noise

The impact of permeability on the trailing-edge noise is analyzed by a constant and a variable porous surface [23]. Porous media generate the Darcy drag force, i.e., the viscous effect of the micro-structure inside a porous medium, which is numerically determined by the permeability and the Forchheimer term. The permeability and the porosity of a baseline configuration are defined based on the acoustic intensity quantified for various porous surfaces [24]. A variable porous medium at a trailing edge is designed by an adjoint-based optimization. The constant and the variable porous medium are applied to two flow configurations, one at zero deg. and one at two deg. angle-of-attack (AOA), to indicate the impact of various loads on the suction and pressure sides on the effectiveness of porous surfaces. In Fig. 6 the directivity determined by the overall sound pressure level is presented. The zero deg. AOA configuration shows that the porous media reduce the noise generation independently from the direction. The acoustic gain is determined by an induced drag force which leads to a lower convection velocity for the turbulent flow passing over the trailing edge. The porous surface is extremely effective to reduce the tone and the broadband noise [24]. The variable porosity configuration shows with the thick arrows an additional noise reduction compared to the constant porosity medium. However, at two deg. AOA the porous surface shows a lower impact on the noise reduction such that the acoustic gain, which is obtained by the optimization at zero deg. AOA is diminished. This sensitivity of the porous-media effectiveness means that in future optimization approaches the AOA should be considered an optimization parameter.

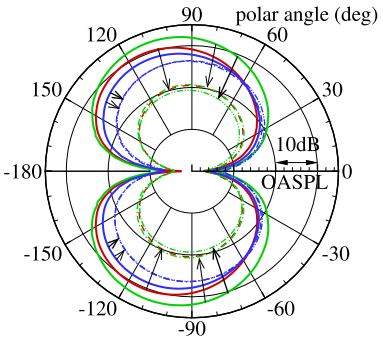

Fig. 6. Overall sound pressure level determined by the acoustic perturbation equations black arrows indicate the noise reduction between impermeable (solid lines) and porous (dashed lines) surfaces color denotes the rounded (red) and the sharp (green) trailing-edge at zero deg. AOA and the rounded trailing-edge at two deg. AOA (blue). (For interpretation of the references to color in this figure legend, the reader is referred to the Web version of this article.)

Written by Seong-Ryong Koh: s.koh@aia.rwth-aachen.de*, Matthias Meinke, Wolfgang Schroeder, RWTH Aachen University, Germany, Beckett Zhou, Nicolas Gauger, TU-Kaiserslautern, Germany.*

2.5. RANS-based trailing-edge noise prediction using Amiet's theory

Küçükosman et al. [25] have recently investigated the accuracy of Amiet's semi-analytical approach [26] for trailing-edge noise prediction when Reynolds-Averaged Navier-Stokes (RANS) simulations are used to determine the wall-pressure statistics. Two families of wall-pressure spectrum models are compared: i) based on a resolution of the Poisson equation by integrating velocity statistics over the boundary layer thickness (Panton & Linebarger model [27]), or ii) directly addressing wall-pressure statistics through ad-hoc empirical models calibrated on experimental databases (Goody, Rozenberg, Kamruzzaman, Catlett, Hu & Herr and Lee models [28]). As illustrative test cases, two different configurations are treated in this work: a NACA0012 airfoil at 0° angle of attack (a.o.a) and a DU96-W-180 airfoil at 4° a.o.a, the key differences between both cases being the importance of the wall-pressure gradient and symmetry between the pressure and suction sides. The results obtained by Küçükosman et al. [25] (see Fig. 7) indicate that both the semi-empirical model developed for adverse pressure gradients and the integral model yield good predictions for the NACA0012 test case. For the Du96-W-180 airfoil, the Lee model which is modified for high adverse pressure gradient flow performs in the range of ±3 dB. The Kamruzzaman model also exhibits a good performance in the range of ±3 dB by considering its simple formulation. Lastly, Panton & Linebarger model predicts well the middle range whereas under-predicts by around 2 dB for the higher frequencies.

Written by Y. C. Küçükosman: yakut.cansev.kucukosman@vki.ac.be*, J. Christophe and C. Schram, von Karman Institute for Fluid Dynamics, Belgium*

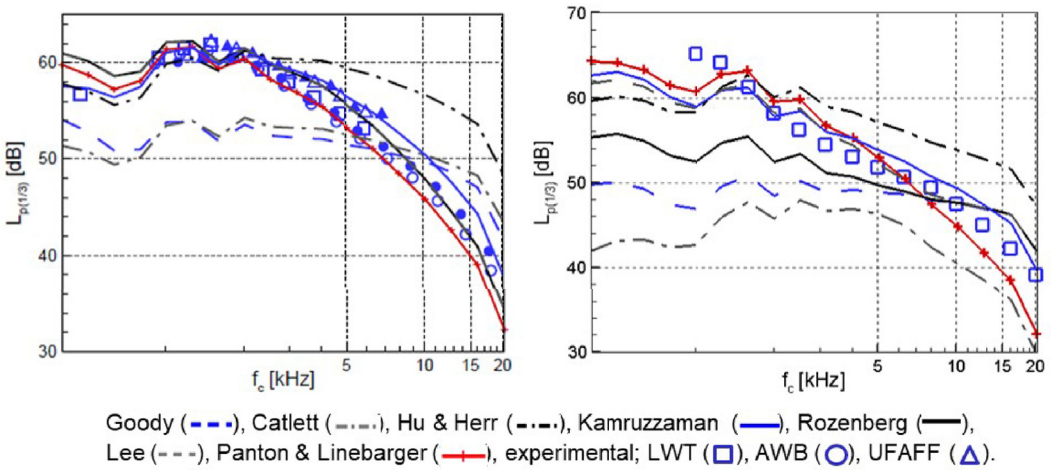

Fig. 7. Far-field noise prediction by Amiet's theory with different wall-pressure models and comparison with an experimental data the NACA0012 airfoil (left) and the DU96-W-180 airfoil (right).

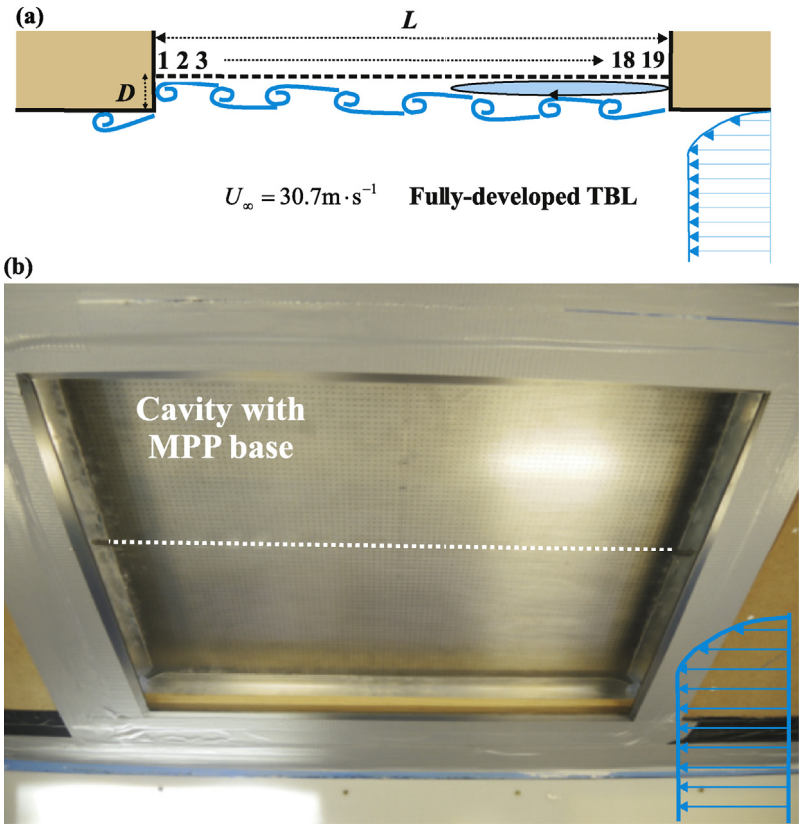

Fig. 8. Views of a transitional flow cavity with micro-perforated base wall beneath a fully developed turbulent boundary layer: (a) sketch of the cavity with numbering of the 19 wall-pressure measurements positions evenly distributed over the centered length line of the base wall (b) photograph of the wind tunnel test section on top of which is mounted the micro-perforated cavity.

2.6. The attenuation of the cavity tones induced by a low-speed flow using micro-perforated panels

Experimental studies have been carried out to assess the effect on the pressure fluctuations of micro-perforating [29] the base wall of cavities mounted in a low-speed wind-tunnel and undergoing a fully-developed turbulent boundary layer [30], as shown in Fig. 8. This passive strategy has hardly been studied in shallow cavities in a transitional flow regime, e.g. with a length-to-depth ratio of about 10. The wall-pressure spectra acquired at Mach number 0.09 over the cavity base panel showed dominant peaks on one third of the cavity floor towards the leading edge. Broadband pressure fluctuations dominate further downstream, with amplitudes of about 10 dB above that of the first peak. The peaks are identified as transverse tunnel-cavity resonances excited by the shear layer and coupled with the thin panel flexural modes. It can be seen from Fig. 9 that micro-perforating the floor of the cavity reduces by up to 8 dB the dominant tonal peaks. This was also observed for a closed-flow cavity, but to a lesser extent. However, the micro-perforations are inefficient downstream of the reduction zone to attenuate the broadband pressure fluctuations, which can even be enhanced. Two-dimensional Lattice-Boltzmann simulations were performed for a transitional cavity mounted in a waveguide and undergoing a low-speed boundary layer. The calculated wall pressure spectra confirmed the existence of transverse tunnel-cavity resonances as well as their attenuation at the base and at the mouth of the cavity by inserting a micro-perforated floor. The dissipation of energy was found to be concentrated within and at the inlet-outlet of the base-wall apertures which correspond to regions of maximum velocity fluctuations. A strategy would be to microperforate only part of the base wall that extends over one third of the cavity length in order to achieve attenuation of the dominant peaks without enhancement of the broadband wall-pressure fluctuations.

Written by Teresa Bravo (teresa.bravo@csic.es), Instituto de Tecnologías Físicas y de la Información, Consejo Superior de Investigaciones Científicas (CSIC), Serrano 144, 28006 Madrid, Spain, and Cédric Maury, Laboratoire de Mécanique et d'Acoustique, UMR 7031 AMU-CNRS-Centrale Marseille, 4 impasse Nikola Tesla, 13013 Marseille, France

2.7. Airfoil noise reduction with add-ons and permeable materials

Leading-edge-impingement (LEI) noise and turbulent-boundary-layer trailing-edge (TBL-TE) noise are amongst the most relevant sources for airframe and turbofan noise (i.e., rotor/stator interaction noise). They can be mitigated by using serra-

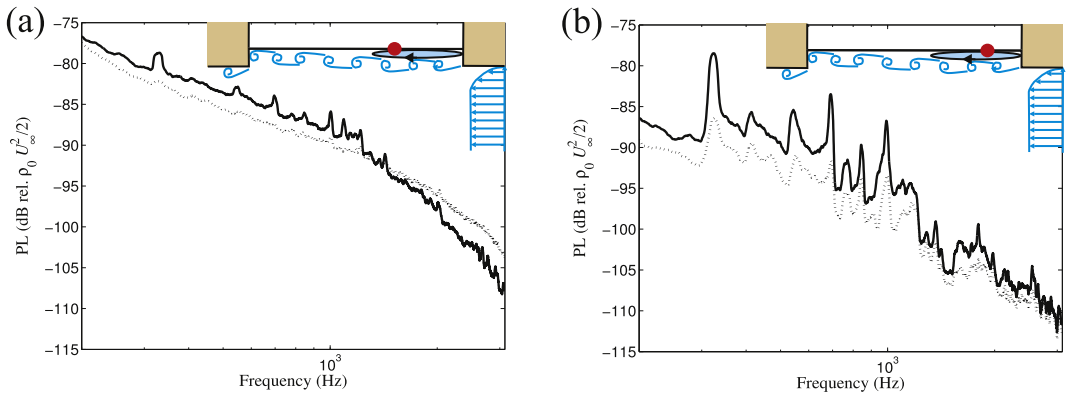

Fig. 9. Effect of a microperforated floor on the pressure level (PL) spectra measured over the base wall of a transitional cavity with length-to-depth ratio 10.6: (a) at 18.2 cm and (b) at 9.8 cm from the cavity upstream edge. The solid curves correspond to a plain floor and the dotted curves to a microperforated floor the red dot in the sketches shows the measurement location. (For interpretation of the references to color in this figure legend, the reader is referred to the Web version of this article.)

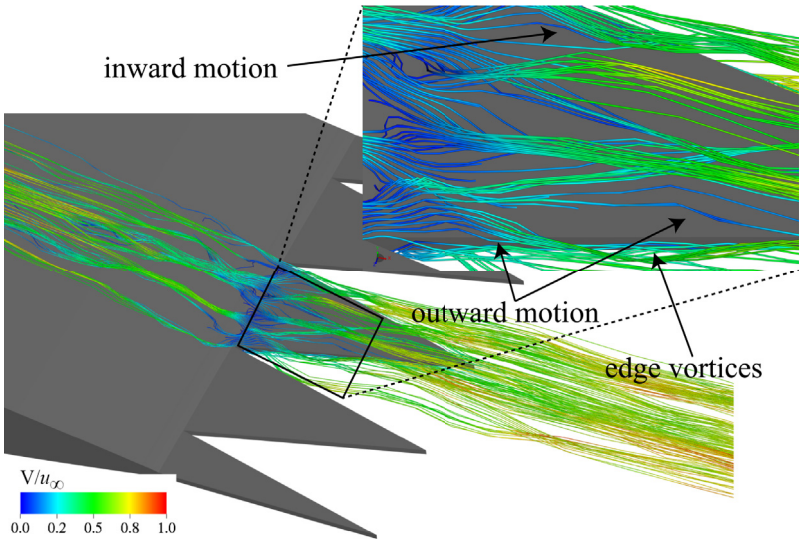

Fig. 10. Streamlines representing the instantaneous flow field over a serrated trailing edge obtained with the Lattice-Boltzmann method.

tions or reducing the pressure imbalance with permeable surfaces. Recent developments have confirmed that serrations reduce noise by generating destructive interference between the scattered pressure waves for both TBL-TE and LEI noise. For TBL-TE noise [31], it has been proven that the effect of the serrations on the flow is to increase the spanwise coherence of the turbulent structures, which promotes destructive interference for slanted edges. This is achieved by altering the flow features over the serration surface, see Fig. 10, both the size of the turbulent structures and their convective direction, as also proved experimentally [32]. Conversely, for rotor/stator impingement noise [33], the dimensions of the turbulent structures in the slipstream of the fan are such that, to realise destructive interference and to reduce noise more than 1 dB, large amplitude serrations are necessary, thus affecting negatively both the aerodynamic performances and robustness of the stator. An alternative approach to reduce noise is the application of permeable surfaces at both the leading and trailing edge. In this case, the noise reduction mechanism is the reduction of the pressure imbalance. For TBL-TE noise [34], permeable materials have been shown to reduce noise up to 10 dB in wind tunnel applications. It has been proven that the conventional model adopted for a solid trailing edge cannot be applied for porous materials because additional noise sources are present. Conversely, for LIN [35], the adoption of a permeable surface at the leading edge has shown that the presence of flow through the insert that forces transition to turbulence, see Fig. 11. In this case, alleviation of LEI noise has been obtained but with an increase of TBL-TE.

Written by F. Avallone (f.avallone@tudelft.nl), D. Ragni, D. Casalino, Delft University of Technology, The Netherlands.

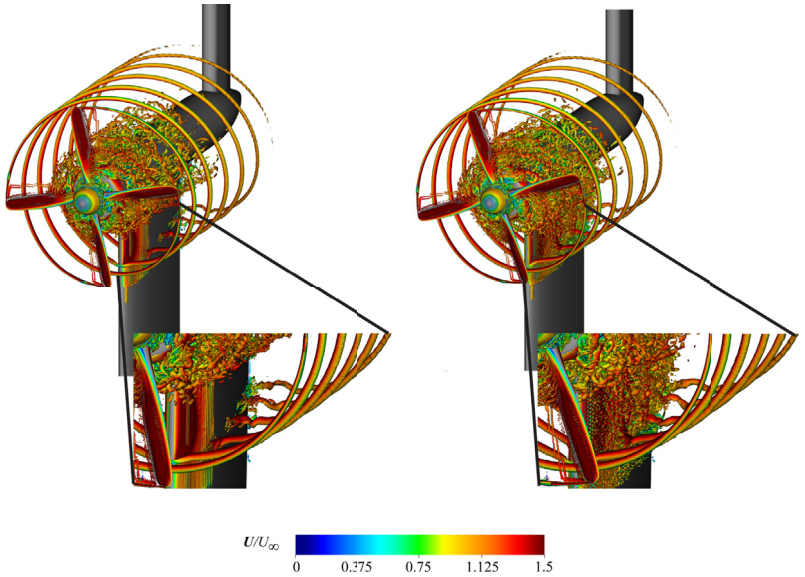

Fig. 11. Instantaneous flow visualisation of the impingement of a propeller slipstream with on a pylon with solid (left) and permeable (right) leading edge.

3. Fan and jet noise

3.1. Shockwave generation and radiation from an UHBR engine with flow distortion using a CFD/CAA chaining strategy

In the framework of the Clean Sky2 ASPIRE project, aeroacoustic investigations were achieved on a full-scale Ultra High Bypass Ratio (UHBR) engine with inflow distortion at transonic conditions [36]. Computational Fluid Dynamics (CFD) simulations were first realized to compute the shocks in the vicinity of the fan, which were then radiated outside of the nacelle thanks to Computational AeroAcoustics (CAA) simulations. The elsA solver [37] was used for both CFD and CAA simulations and the coupling was done by injecting the shocks in terms of usual conservative variables using a non-reflecting boundary condition [38]. The CAA solver is based on the non-linearized Euler equations which allow to define the CFD/CAA interface close to the fan where the propagation of shocks is highly non-linear. Both shock generation and shock propagation mechanisms were investigated and the effects of inflow distortion were highlighted by comparison with a baseline case without distortion. It was shown that the distortion, characterized by an acceleration of the flow at the bottom of the nacelle (Fig. 12), is responsible for a modification of the shock amplitudes that depends on the circumferential position. Thus, azimuthal modes appear in addition to the rotor-locked mode present without distortion. The near-field radiation is highly impacted with most of the noise being directed towards the sky (Fig. 13). This is shown to be caused by the blockage of shocks by a supersonic flow region in the

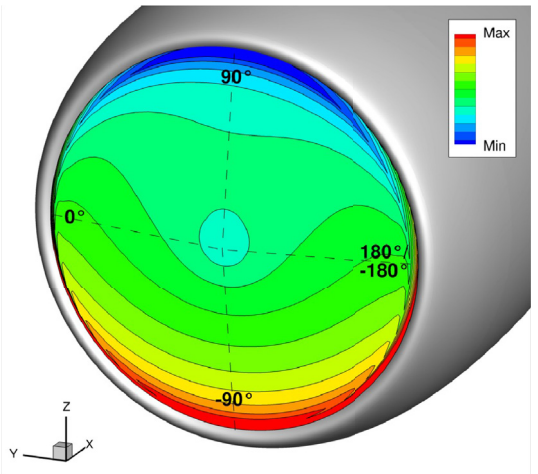

Fig. 12. Inflow distortion map (axial velocity contours).

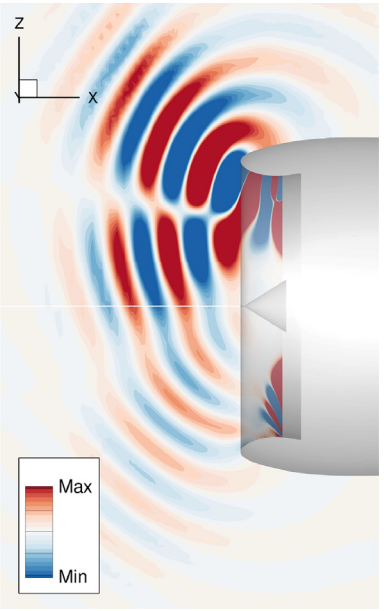

Fig. 13. Pressure radiated through the inlet at the BPF (vertical plane).

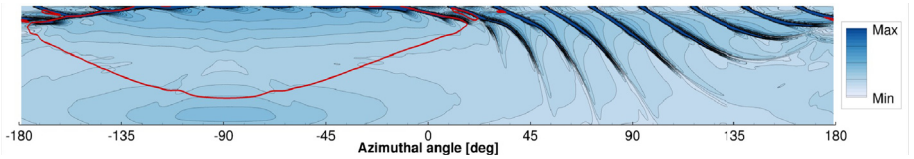

Fig. 14. Instantaneous density gradient magnitude contours and sonic isoline (in red) in the inlet (unwrapped radial slice, the fan is at the top, the nacelle entrance is at the bottom). (For interpretation of the references to color in this figure legend, the reader is referred to the Web version of this article.)

bottom of the nacelle (Fig. 14). ONERA carried out this study in close cooperation with partners Airbus, NLR, and DLR and received funding from the Clean Sky 2 Joint Undertaking under the European Union's H2020 program (grant agreement no. 681856).

Written by M. Daroukh: majd.daroukh@onera.fr, *C. Polacsek, A. Chelius, ONERA - The French Aerospace Lab, Châtillon, France.*

3.2. A novel facility for the investigation of fan noise generation mechanisms: ECL-B3

The fan module is expected to be the major noise source of future Ultra-High-Bypass-Ratio (UHBR) turbofan engines. Among the reasons are the increase in fan diameter, a reduction of the exhaust jet speed and the shortening of the nacelle. The new ECL-B3 test rig shown in Fig. 15 is dedicated to advanced research in aeroacoustics [39] as well as aero-dynamic and aero-elastic instabilities of fan stages [40]. This facility, the result of a collaboration between the Fluid Mechanics and Acoustics Laboratory and Safran Aircraft Engines, was inaugurated in 2018 at the Ecole Centrale de Lyon. The first tested configuration was a scaled modern UHBR fan manufactured by Safran Aircraft Engines within the ENOVAL European project. The noise generated by the fan module was measured by in-duct wall-flush mounted microphones intended for the characterization of the modal content. Some of the sensors are mounted on rotating rings allowing a fine spatial discretisation. The angular steps have been optimized such as to minimise the number of rotating steps while keeping modal basis parameters such as the mutual coherence and condition number as low as possible over a wide frequency band. The invariably lost phase relationships between probes at the sequential positions are reconstructed. Fixed reference microphones have been used to estimate the complete cross-spectral matrix as if measurements at sequential steps were recorded simultaneously. Modal amplitudes are estimated by using an iterative Inverse Bayesian Approach [41]. The resulting algorithm allows to control the degree of sparsity imposed on the solution. For instance, at tonal frequencies the number of dominant modes is expected to be small due to constructive interferences, a high degree of sparsity is appropriate. For broadband noise, a mild sparsity assumption would be more pertinent [39].

Written by Antonio Pereira: antonio.pereira@ec-lyon.fr, *Laboratoire de Mécanique des Fluides et d'Acoustique, Ecole Centrale de Lyon, France, Mathieu Gruber, Safran Aircraft Engines, France.*

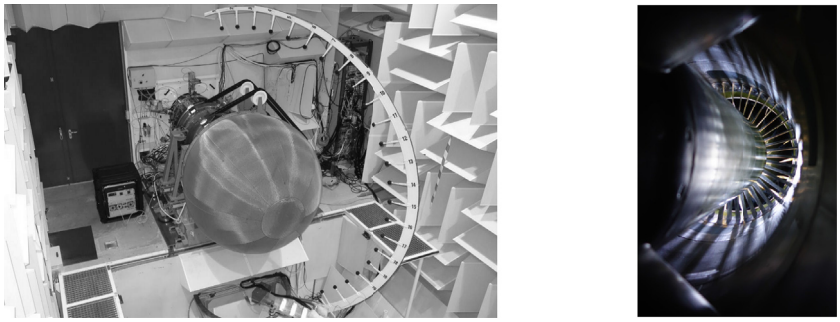

Fig. 15. Left, view of the Turbulence Control Screen (TCS) and the traversable microphone array for directivity measurements in the anechoic chamber of the ECL-B3 facility. Right, in-duct view from the downstream test section showing stator vanes.

3.3. Multi-port eduction of installation effects applied to a small axial fan

In HVAC systems, the noise emitted by the fan is usually characterized in a test bench ensuring a relatively ideal constant and uniform inflow. In contrast, the implementation of this fan in an industrial duct system will often result in a non-uniform and unsteady flow field due to the presence of nearby bends, valves, etc. Those distorted inflow conditions are usually accompanied by an increase in noise emissions [42]. An experimental investigation of aeroacoustic installation effects was performed in the ALCOVES (Aeroacoustic Lab for COoling and VEntilation Systems) test bench of the von Karman Institute for Fluid Dynamics [43] for the case of an axial fan such as found in domestic appliances. A multi-port methodology [44] has been used to extract the active noise emitted by the fan in various inflow conditions, by decontaminating the microphone measurements from the test bench acoustic reflections and turbulent boundary layer pressure fluctuations. The inflow distortions were shown to have a strong impact on the acoustic emissions and aerodynamic performance of the fan. Using similarity laws, it was shown that the alteration of the operating point is not sufficient to explain the impact of distorted inflows on the acoustic power radiated by the fan. The broadband noise, in particular, was shown to be very sensitive to the turbulence shed by the grids, with additional noise of the order of 10 dB at some frequencies in Fig. 16. The results suggest the need for novel acoustic design guidelines accounting for inflow quality in addition to the classical indicators solely based on the performance point.

Written by Joachim Dominique (Joachim.dominique@vki.ac.be), Christophe Schram, Julien Christophe, von Karman Institute, Belgium and Raul Corralejo (raul.corralejo@dyson.com), Dyson Ltd, Malmesbury, England.

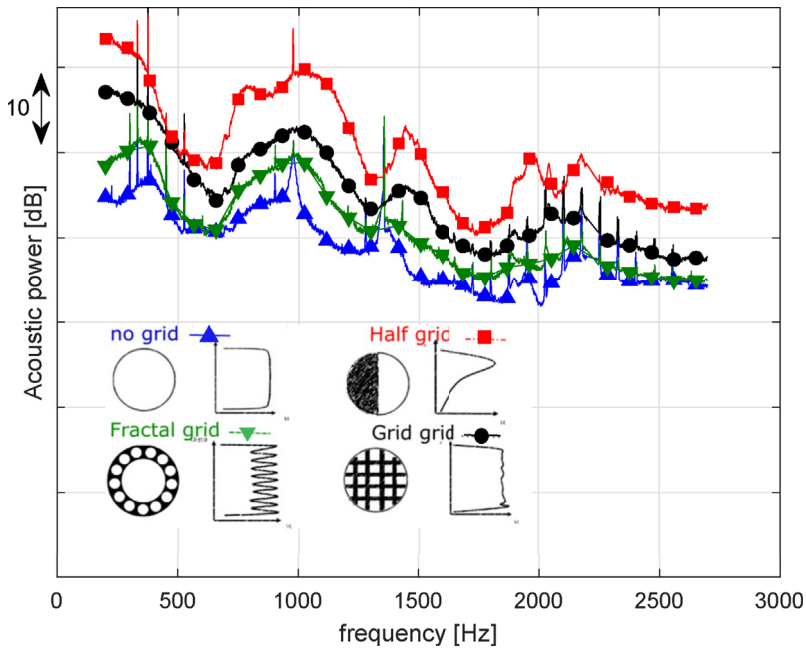

Fig. 16. Acoustic power upstream of the fan under different inflow conditions at the same rotational speed.

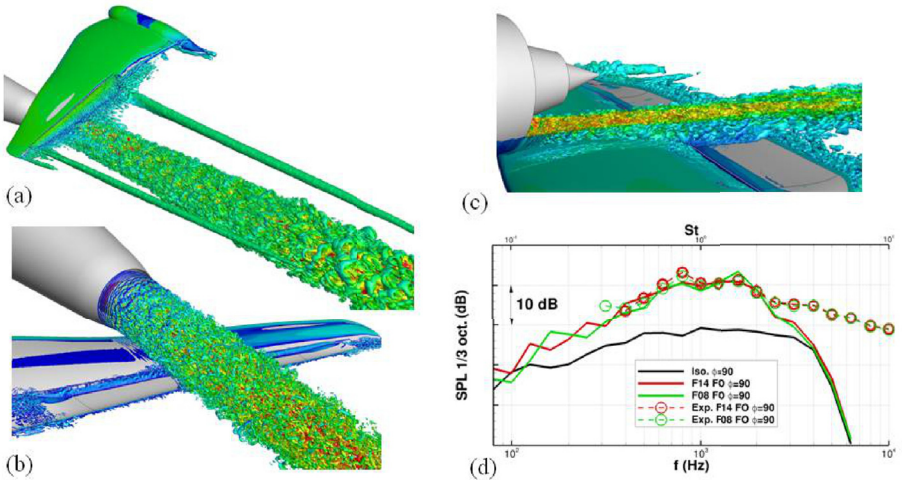

Fig. 17. (a–c) Jet flow and interaction with wing-flap geometry, (d) isolated (Iso.) and installed sound pressure level for flap deflections 8 (F08) and 14 (F14) degrees with measured (Exp.) data.

3.4. Prediction of far-field sound of installed complex geometry ultra-high bypass ratio jets in flight using LES

Growing aero-engine bypass ratios means the noise directly generated by the jet has now decreased significantly. Another consequence is that the relative importance of installation noise has increased. Increasing engine diameters can lead the jet to directly interact with the wing and flap generating significant noise sources. Using LES in a blind test, flow and resulting far-field sound has been accurately predicted for complex geometry installed configurations under flight conditions [45]. This is difficult and costly to adequately achieve experimentally, yet well defined numerically. Fig. 17 shows the jet-wing-flap interaction and far-field sound directly below the aircraft. Agreement with available measured sound data is clear. Isolated and installed configurations, have been contrasted for round nozzles with two flap deflections [45] and nozzles with serrations [46]. For round nozzles, a 20 dB increase in noise was predicted and greatly reduced with nozzle serrations. This is due to increased turbulence dissipation reducing jet-flap interaction. Using high-fidelity unsteady data sets, noise sources and their distribution have been identified [45]. Furthermore, turbulence length and time scale distributions have been calculated [45,47] to inform lower fidelity modelling such as RANS, that can be used to guide rapid design tools. A modelling framework has been defined for complex geometries [45] consisting of modular hybrid structured-unstructured mesh generation, low dissipation numerical discretisation, hybrid LES-RANS turbulence modelling, Ffowcs Williams-Hawkings (FW-H) surface generation and far-field propagation [45]. The same procedure has recently been successfully validated in another blind test for large scale simulations including a pylon and fuselage. This highlights the ability of the approach to reliably replace significant amounts of rig testing, also providing greater consistency.

Written by J C Tyacke: james.tyacke@ brunel.ac.uk, *Brunel University, UK (reported work undertaken at the Department of Engineering, University of Cambridge)*

4. Helicopter noise

4.1. Blade-vortex interaction noise controller based on Miniature Trailing Edge Effectors

A methodology to suppress/alleviate the noise annoyance emitted by blade–vortex interaction (BVI) phenomena occurring on helicopter main rotors developed and validated in Refs. [48,49] has been presented. The proposed methodology is suitable for the identification of multi-cyclic harmonic controllers based on the actuation of rotor blades equipped with Miniature Trailing Edge Effectors (MiTEs). The low-power requirements make MiTEs particularly suited for this kind of application. The objective of the control methodology is the direct suppression of the aerodynamic noise sources by the generation of localized high-harmonic unsteady aerodynamic loads (as much as possible equal and opposite to those produced by BVI phenomena) aimed at cancelling out those caused by the BVI events. The set-up of control devices is selected on the basis of the blade-vortex interaction scenario, taking into account a trade-off between effectiveness and power requirement. The control law is efficiently identified by means of an optimal controller synthesized through suitable two-dimensional multi-vortex, parallel blade-vortex interaction problems. The proposed methodology is validated by the application to realistic helicopter main rotors during low-speed descent flights, numerically simulated through high-fidelity aerodynamic and aeroacoustic solvers based, respectively, upon a three-dimensional free-wake boundary element method [50] for the solution of potential flows around rotors in blade-vortex interaction conditions and the Farassat 1A formulation. Results demonstrate that the proposed control approach is a promising method to reduce BVI noise.

Written by S. Modini (saramodini@gmail.com), G. Graziani, University of Rome Sapienza, Italy and M. Gennaretti, G. Bernardini, Roma Tre University, Italy).

4.2. Rotorcraft comprehensive code assessment for blade-vortex interaction conditions

Computational methodologies applied to a comprehensive code for rotorcraft developed in recent years at Roma Tre University are presented in Ref. [50], along with an assessment of its prediction capabilities focused on flight conditions characterized by strong blade-vortex interaction phenomena. This comprehensive code includes a detailed aeroelastic response analysis of the blade within the trim procedure: a three-dimensional, potential-flow, a rotor aerodynamics solver which is fully coupled with a bending-torsion beam model of blade structural dynamics, and a harmonic-balance/modal approach is used to integrate the rotor aeroelastic equations [51]. Hence, for a prescribed flight condition, the aeroelastic trim module provides pitch control settings and vehicle attitude, blade elastic response, mean and vibratory hub loads, as well as the pressure distributions required to define the noise sources in the aeroacoustic module. The rotor noise radiation is evaluated through the widely-used boundary integral Farassat 1A formulation. The validation campaign of the comprehensive code has been carried out against the well-known HART II database, which is the outcome of a joint multi-national effort aimed at performing wind tunnel measurements of loads, blade deflection, wake shape and noise concerning a four-bladed model rotor in low-speed descent flight. Comparisons with numerical simulations available in the literature for the same test cases are also presented. It is shown that, with limited computational cost, the results provided by the Roma Tre aero-acousto-elastic solver are in good agreement with the experimental data, with a level of accuracy that is in line with the state-of-the-art predictions. The influence of the vortex core modelling on aerodynamic predictions and the influence of the inclusion of the fuselage shielding effect on aeroacoustic predictions are discussed.

Written by M. Gennaretti: massimo.gennaretti@uniroma3.it, G. Bernardini, J. Serafini, University Roma Tre, Italy and G. Romani, Delft University of Technology, The Netherlands

5. Aircraft interior noise

5.1. Parametric study on effects of wall pressure wavenumber spectra on aircraft fuselage vibration

The wall pressure wavenumber spectra in the front region of the aircraft fuselage at cruise condition are formulated based on the wall pressure cross-spectral model [52]. The formulated spectra are used as excitation sources for the calculation of the fuselage panel vibration with the Statistical Energy Analysis method [53]. The coherence length, the convection velocity and the flow angle are modified to study their effects on the wavenumber spectrum and the panel vibration. Furthermore, the practical impact of parametrically important factors on the calculated results such as the surface microphone array size and resolution, window functions and dealing with noisy signals is studied, see Ref. [54]. Figs. 18 and 19 show the effect of coherence length and convection velocity modifications on the wavenumber spectra and the panel vibration. For the frequencies between 800 Hz and 2 kHz in which a possible coincidence between the flow excitation and the panel vibration occurs, the wavenumber spectral peak region is important for the excitation. A change in the spectral peak level results in a respective change in panel vibration level. For frequencies outside of 800 Hz–2 kHz, the lower streamwise wavenumber spectral range is important for the excitation. Figs. 20 and 21 show the effect of the array size, resolution and noise. A too small resolution or a too small size will strongly affect the calculated wavenumber spectra and vibration. However, an overly large array size will increase the error due to a reduction of the signal-to-noise ratio when dealing with noisy signals.

Written by Nan Hu: nan.hu@dlr.de, DLR, Germany, Sören Callsen, Airbus Operations GmbH, Germany

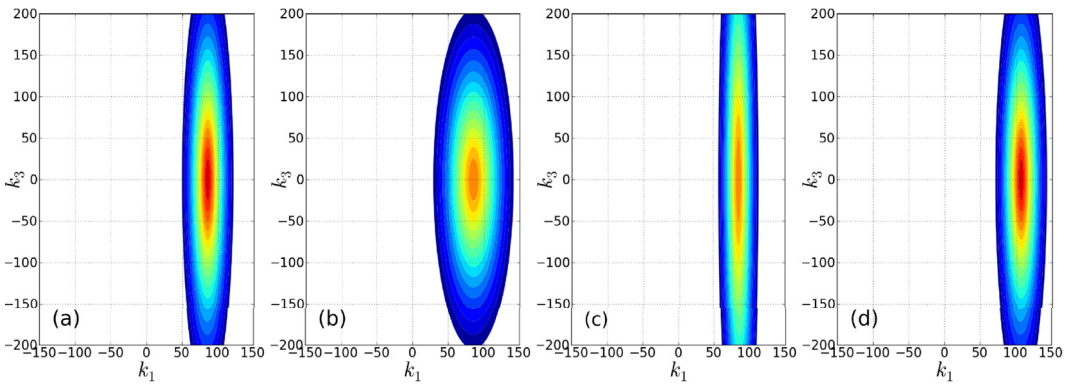

Fig. 18. Contour plot of wavenumber spectra at 2500 Hz with levels between −54 dB and −35 dB (a) Smol'yakov model (b) 0.5 l_1 (c) 0.5 l_3 (d) 0.8 u_c.

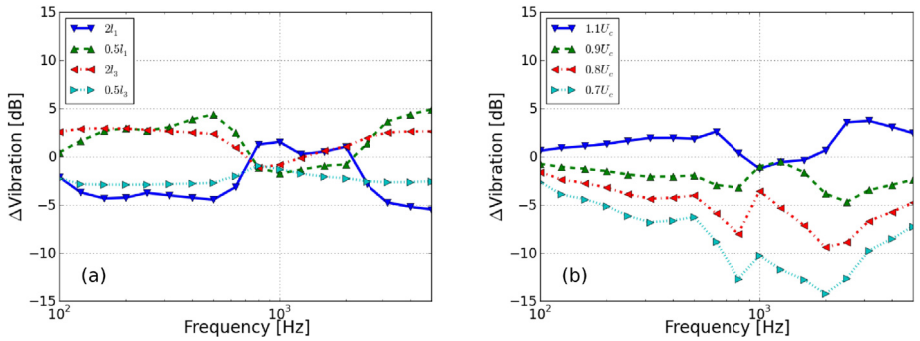

Fig. 19. Comparison of panel vibration (a) modification of coherence lengths (b) modification of convection velocities.

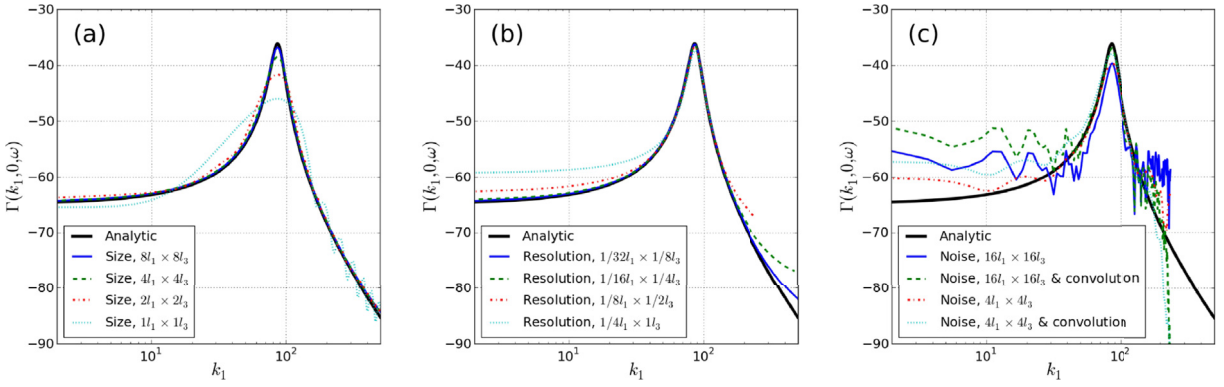

Fig. 20. Comparison of streamwise wavenumber spectra at 2500 Hz with different processing settings (a) array sizes (b) array resolutions (c) noisy signal.

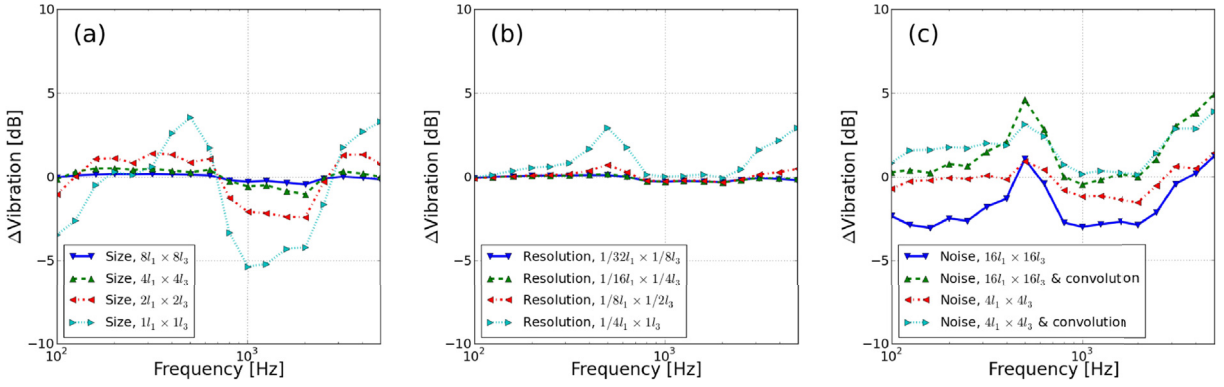

Fig. 21. Comparison of panel vibration with different processing settings (a) array sizes (b) array resolutions (c) noisy signal.

6. Propeller noise

6.1. Contra-rotating open rotors (CROR) as a viable aircraft propulsion system: experimental, numerical and analytical studies

Noise from contra-rotating open rotors is a major obstacle to the adoption of this fuel-efficient technology as a viable aircraft propulsion system. A better understanding of both contra-rotating open rotor noise generation, reduction and shielding has been achieved recently due to ongoing research based on the WENEMOR data [55–57] where 288 test conditions of a 1:7 scale green regional aircraft model were completed. A wide range of airframe configurations equipped with two installed CROR engines operating in both pusher and tractor modes and operated at both approach and takeoff settings were assessed as a function of wind tunnel speed and angle of attack. The geometric parameters which were varied included interchangeable tailpieces (T, L and U empennage), variable fuselage length, engine pylon rotation, and engine pylon elongation and these allowed shielding

effects, pylon wake effects as well as the benefits to be gained from moving the entire CROR out of the wing wake to be assessed [58]. In addition to the full installation analysis set-up, a second campaign was conducted where only the installed-on-pylon contra-rotating open rotor configuration was evaluated [59]. The experimental results were used to validate an original numerical method for the calculation of engine noise installation effects and its application to contra-rotating open rotor propulsion was demonstrated. This method is based on the weak coupling between computational fluid dynamics, an integral method based on Lighthill's analogy for the calculation of acoustic radiation, and on a boundary element method for the calculation of the acoustic diffraction by the aircraft fuselage and empennage [60,61]. In addition, the equal number of blades fore and aft for the CROR engines considered, has provided interesting opportunities such as a study which approaches the question of counter-rotating open rotor engine noise levels from a yet unexplored perspective, examining the radiation efficiency properties of unducted turbomachinery acoustic modes in order to provide design guidelines that mitigate the radiation of sound without the need for shielding [62].

*Written by Gareth J. Bennett (*gareth.bennett@tcd.ie*) and John Kennedy (*kennedj@tcd.ie*), Trinity College Dublin, the University of Dublin. Ireland*

7. Techniques and methods in aeroacoustics

7.1. The conditions of quadrupole moment conservation in the evolution of small perturbations of stationary flows

Perturbations of incompressible ideal fluid flows are described in terms of the Lagrangian and Hamiltonian formalism [63]. Expressions for the Lagrangian and Hamiltonian in which the displacement field and momentum density perturbation field are used as canonical variables are obtained. Based on Noether's theorem, the conditions of conservation of the quadrupole moment of perturbations of the flow are derived. It is shown that these conditions are satisfied for any uniform jet flows both in the two- and three-dimensional cases. The results are of great importance in aeroacoustics because the quadrupole moment of the flow is the principal term of acoustic source expansion in the Mach number. Conservation of the quadrupole moment means that the evolution of perturbations of uniform jet flows under arbitrary initial conditions makes no contribution to quadrupole sound radiation in the linear approximation. Therefore, sound sources of low-velocity jets may be related to finer effects, such as weak non-uniformity of the flow in the streamwise direction or nonlinearity of perturbations. It is also possible that the idea that sound sources in a turbulent jet are small perturbations on the background of the mean flow does not correspond to their real nature and generation of acoustic perturbations in the turbulent flow is significantly affected by the local non-linear structure of the vorticity.

*Written by Sergey Chernyshev (*slc@tsagi.ru*) and V.F. Kopiev (*vkopiev@mktsagi.ru*), TsAGI, Russian Federation.*

7.2. Noise reduction of VEGA launch pad environment at lift-off

In 2015, ONERA performed the analysis of microphone array data measured during VV05 of VEGA launcher in Kourou, on behalf of ESA [64]. Approximately at the payload fairing level, a 2 m diameter circular array composed of 32 microphones, was implemented on one of the anti-lightning pylons, oriented toward the exhaust duct, aimed at identifying the location and level of the acoustic sources generated during lift-off. Based on this study, the contributions to the overall noise from the engine jet, the table and the flame trenches were highlighted and as a trade-off between acoustic benefits and costs, ESA decided to modify the launch table by closing existing openings with heavy steel plates filled with porous materials. Two years later, in 2017, during VV10, the same microphone array measurements were realized. Direct comparison of the acoustic levels measured on the microphones pointed out a reduction of about 2 dB at the frequencies of interest, and even more for higher frequencies. A deconvolution method developed in ONERA [65], based on the well-known DAMAS [66], was applied to three scanning plans, including a total of about 3000 sources. When the launcher is at the lowest altitudes, corresponding to the most critical moment for acoustics, the source localization confirmed a strong reduction of the sources radiated from the table, with only a slight change from the flame trenches (Fig. 22). More recently, in 2018 [67], the final step consisted of propagating the acoustic sources

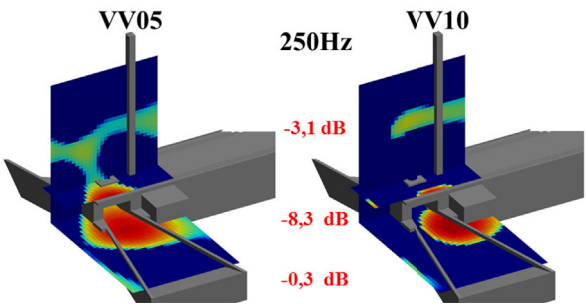

Fig. 22. Acoustic reduction on each scanning plan at 0 m.

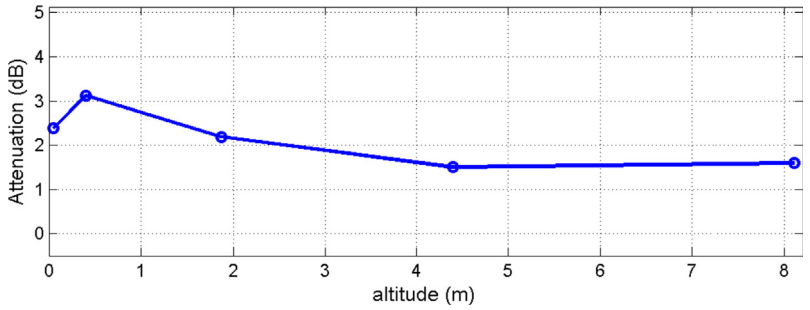

Fig. 23. Acoustic attenuation at the fairing level – Evolution with the altitude.

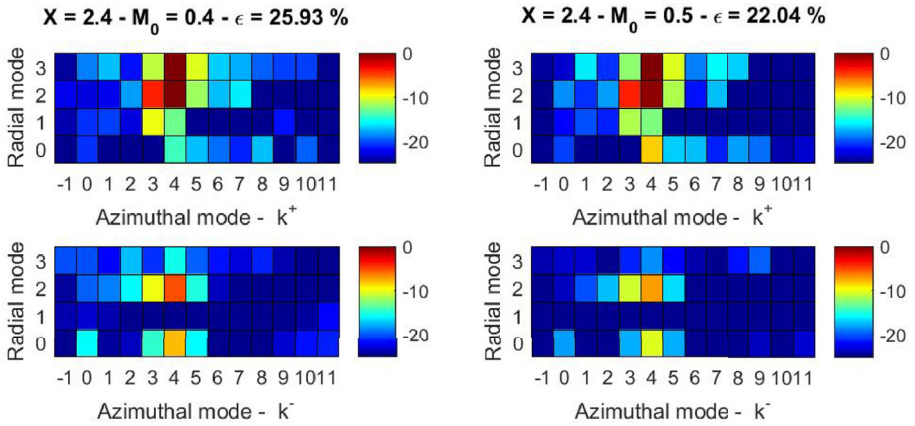

Fig. 24. Normalized power cross spectral matrix of the amplitude of the modes obtained by correlated ARMADA on the bypass duct @BPF2, considering $M_0 = 0.4$ (left) and $M_0 = 0.5$ (right).

to the fairing. As the microphone array is in front of one of the two ducts, the reasonable hypothesis that they generate similar noise (uncorrelated) is made and the sources identified on the flame trench are symmetrized. Diffraction effect on the fairing is taken into account thanks to the correction of an infinite cylinder. The results (Fig. 23) are coherent: the effect of the table covers progressively decreases with the increasing distance of the launcher from the pad, leading to a corresponding reduction of the acoustic benefit.

Written by F. Cléro: franck.clero@onera.fr, *F. Mortain, ONERA - The French Aerospace Lab, France, D. Palmieri, ESA-ESRIN, Italy*

7.3. Duct azimuthal and radial modal deconvolution of CFD analysis of UHBR engine tonal noise

A modal deconvolution method is used to characterise the main propagating acoustic duct modes from non-intrusive measurements. In the framework of the ASPIRE-CS2 project, ONERA's modal deconvolution method ARMADA [68] is applied to numerical data from a generic UHBR engine at the take-off sideline condition. The numerical simulation is provided by NLR to quantify the tonal internal acoustic field by the application of a CFD approach for the configuration with a clean fan channel [69]. The complex geometry of the nacelle implies a variable Mach number through the fan duct, which is unfortunately not precisely known. As a first step, an azimuthal Fourier transform is applied to determine the content of the dominant azimuthal modes. In the bypass duct (downstream direction), they are shown to be quite constant, whereas, upstream from the fan, they vary significantly in the vicinity of the inlet. Therefore, our deconvolution method [68], extended to an annular duct, is only applied on the bypass duct, using data obtained at BPF2 on the wall as it would be for flush mounted microphones. We consider a modal basis restricted to azimuthal mode orders from −1 to 11, which is relevant to explain the main content of the total sound pressure. Considering a constant flow rate with two hypotheses of Mach number (0.4 and 0.5), and under the correlated mode assumption, the results explain more than 74% of the data. The more energetic modes correspond to azimuthal mode m = 4 and radial modes n = 2 and 3, together with m = 3 and n = 2; they are found to be perfectly correlated. Modes propagating in the upstream direction (k^-) point out possible reflections at the end of the nacelle (see Fig. 24).

Finally, the acoustic pressure field (absolute value of the Fourier transform) is reconstructed from the estimated modes (cross-spectral matrix of the amplitude), and compared to the initial numerical data (see Fig. 25). The black frames highlight

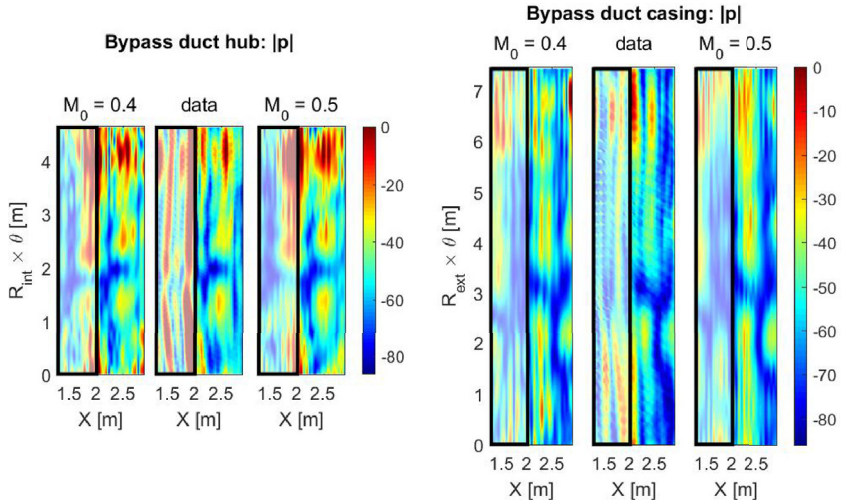

Fig. 25. Absolute value of the Fourier transform of the pressure field reconstructed on the bypass duct hub surface (left) and duct casing surface (right).

areas where some modes, not included in the modal basis, go from cut-on to cut-off. Using only data obtained on the wall, ONERA's deconvolution method succeeds in providing a good representation of the acoustic field in the bypass duct.

Written by S. Fauqueux: Sandrine.Fauqueux@onera.fr, *ONERA - The French Aerospace Lab, Aerodynamics Aeroelasticity Acoustics Department, Châtillon, France*

7.4. Uncertainty quantification for direct aeroacoustics of cavity noise

Cavity noise has become a major concern in automobile exterior aerodynamics. Different noise generation mechanisms have been identified, such as Helmholtz resonance, standing waves and Rossiter feedback, which all lead to tonal noise emission. Both frequencies and sound pressure levels of cavity noise are highly sensitive to geometric and environmental uncertainties. Those sensitivities can lead to deviating results between experiment and numerical simulations. Uncertainty quantification (UQ) is, therefore, a promising tool to gain deeper insight into the factors influencing the sound spectra. A UQ framework based on the deterministic high-order discontinuous Galerkin solver FLEXI has been developed to quantify the influence of random input parameters on cavity noise. UQ was realized through a non-intrusive spectral projection method which revealed fast stochastic convergence in comparison to sampling-based methods. With the help of this framework, the system response of a cavity flow problem under the influence of uncertain parameters has been analyzed. Uncertainties in the upstream boundary layer as well as randomness in the cavity geometry have been investigated [70]. As an example, the acoustic response to an uncertain cavity depth revealed strong non-linearities. For a given critical cavity depth, sudden mode switching of the first two dominant Rossiter modes and the associated distinct frequencies has been identified (Fig. 26a). The resulting pressure spectrum provided the stochastic noise production which included all dominant, unstable modes and can be interpreted as the superimposition of two distinct feedback regimes (Fig. 26b).

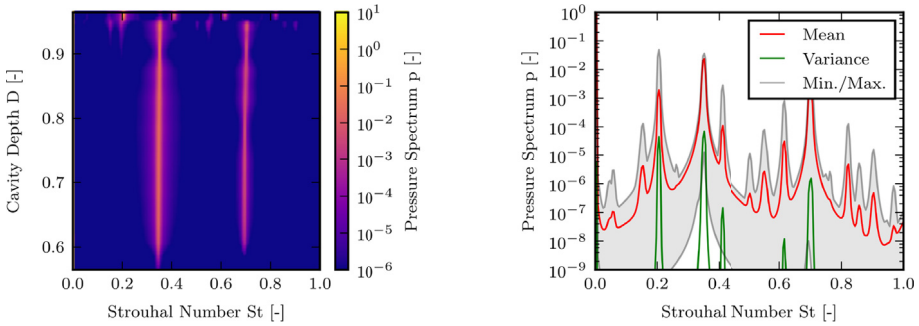

Fig. 26. Influence of an uncertain cavity depth D on aeroacoustic feedback. Response surface plotted as a Campbell diagram (a). Stochastic pressure spectrum with expectation and variance (b).

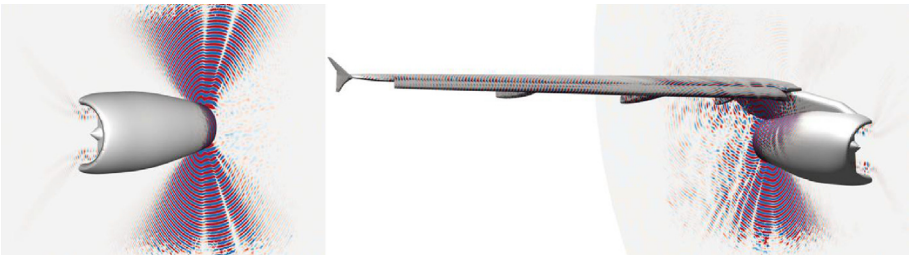

Fig. 27. Sound pressure of the isolated (left) and installed (right) engine cases.

Written by Thomas Kuhn (thomas.kuhn@iag.uni-stuttgart.de), Daniel Kempf and Claus-Dieter Munz, Institute of Aerodynamics and Gas dynamics, University of Stuttgart, Germany

7.5. Simulating tonal fan noise of an aircraft in flight

To ensure compliance with noise regulations, expensive fly-over tests are needed. No numerical alternative currently exists. Yet an accurate "virtual fly-over" would revolutionize the design process of future aircraft as it can help to assess the most relevant noise sources at an early design stage. As a first step towards enabling such a "virtual fly-over", Mößner et al. [71] developed a method capable of studying tonal rotor-stator-interaction noise from its generation in the fan stage to its propagation to observer positions at ground level. Solving this problem with a single, high-fidelity method is hardly realizable, particularly in terms of computation costs. Instead, a computational chain consisting of multiple high-fidelity methods was established. The entire task was split into smaller subtasks that can be handled by specialized tools with the aim of performing each subtask as accurately and efficiently as possible. Different subtasks include the fan noise generation, the propagation in the bypass and inlet ducts and the shielding and scattering effects due to the engine's installation. Special care was taken to validate the accuracy of the interfaces between the tools. To ensure that the entire computational chain delivers plausible results, the results were compared to another simulation [72] using an established technique for the case of an isolated engine and a good agreement was found. To prove the new method's capability of predicting the tonal fan noise of an installed engine, the technique was applied to a V2527 engine mounted underneath the fully equipped wing of an A320 aircraft in approach conditions (shown in Fig. 27). In Fig. 28, the acoustic footprint on the ground is shown for the isolated and installed engine cases. For the installed engine, scattering effects cause a complex interference pattern. The overall magnitude of sound pressure level and general directivity of the installed and isolated engine cases is, however, comparable for the investigated configuration. In summary, the efficiency of the method as well its capability for computing complex scattering effects were demonstrated. In future investigations, it is essential to incrementally increase the complexity of the simulation to pinpoint the most relevant noise mechanisms of fly-over tests.

Written by C. Kissner: carolin.kissner@dlr.de, M. Mößner, J. Delfs, L. Enghardt, German Aerospace Centre (DLR), Germany.

7.6. Enhanced HR-CLEAN-SC for resolving multiple closely-spaced sound sources

Enhancement of spatial resolution in acoustic imaging has been obtained by using an optimized acoustic array together with the Enhanced high-resolution (EHR) CLEAN-SC algorithm [73]. The EHR-CLEAN-SC algorithm is based on the well-known CLEAN-

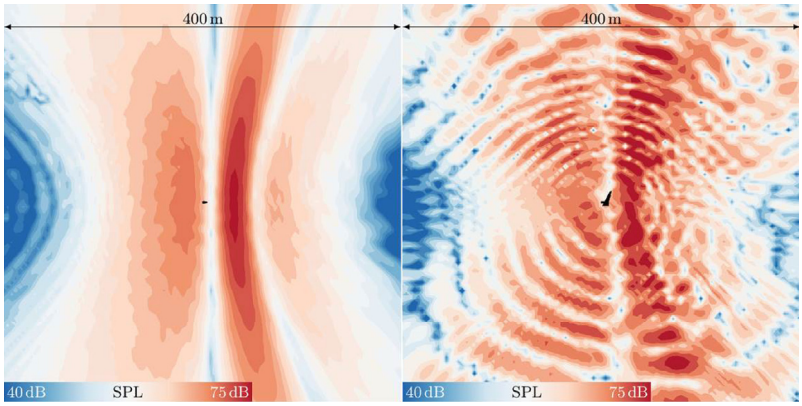

Fig. 28. Acoustic footprint of the isolated (left) and installed (right) engine configurations.

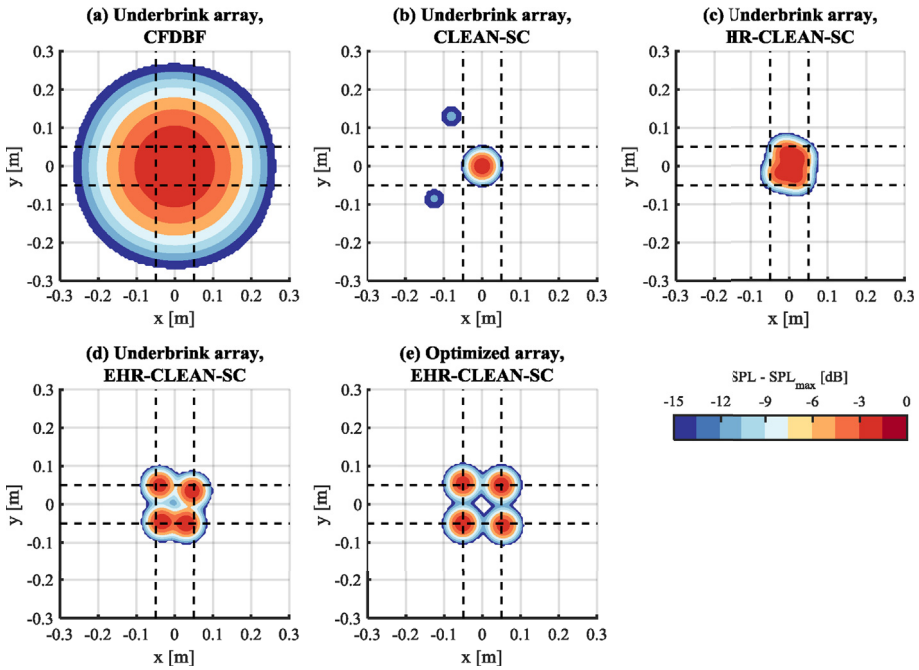

Fig. 29. Source maps showing the sound pressure level relative to the maximum sound pressure level (SPL-SPLmax) of four synthesized sound sources with 10 cm separation produced by using the 'Underbrink array' and (a) CFDBF, (b) CLEAN-SC, (c) HR-CLEAN-SC, and (d) EHR-CLEAN-SC, compared with the same source setting resolved by EHR-CLEAN-SC with the optimized acoustic array (e) at 1.8 kHz (The sources are at the intersections of the dashed lines.

SC algorithm [74] that provides clean source maps in which sidelobes that are spatially coherent to the sources are eradicated. Still, the resolution of CLEAN-SC is limited by the Rayleigh criterion. The HR-CLEAN-SC algorithm [75] surpasses this limit, by explicitly accounting for the presence of closely-located sources. To find the locations of these sources, the source markers are relocated away from the peak in the source map, to a location where the combined influence of the other sound sources is minimal. The freedom of the source marker relocation is limited by the sidelobe level. A first step to enhance the HR-CLEAN-SC performance is to ensure low sidelobe levels by optimizing the array design. Secondly, the source marker relocation is done such that it exploits the low-sidelobe design of the acoustic array. It was demonstrated that the resulting EHR-CLEAN-SC algorithm could resolve four closely-spaced sound sources down to more than half the frequency set by the Rayleigh criterion, using both synthetic and experimental data [73]. An example is shown in Fig. 29 presenting the source maps of four closely-spaced synthetic incoherent sound sources and using the standard 'Underbrink array'. In subplots a to d, the results are shown for conventional frequency-domain beamforming (CFDBF), CLEAN-SC, HR-CLEAN-SC, and EHR-CLEAN-SC. Subplot e shows the results when the optimized array is used together with the EHR-CLEAN-SC algorithm. The maps are shown at a frequency of 1.8 kHz, while, according to the Rayleigh criterion, the sources are expected to be resolved only above 4.2 kHz. In practice, the EHR-CLEAN-SC algorithm is recommended for examining closely-spaced aeroacoustic sound sources such as landing gear noise [76].

Written by S.Luesutthiviboon: s.luesutthiviboon@tudelft.nl*, A.M.N. Malgoezar, R. Merino-Martinez, M. Snellen, P. Sijtsma, D.G. Simons, Section Aircraft Noise & Climate Effects (ANCE), Faculty of Aerospace Engineering, Delft University of Technology, The Netherlands.*

7.7. Statistical inference method for liner impedance eduction with a shear grazing flow

Understanding the effects of a complex flow on the acoustical response of nacelle liners is of prime importance for current nacelle liner design. The acoustical response of a liner is characterized by its impedance ζ, whose measurement, in the presence of a grazing flow, can be achieved through indirect "eduction" methods. These methods consist of matching an experimental observation to a numerical simulation, via an optimization procedure. In practice, either the pressure field is measured on the wall opposite the liner [77], or the velocity field is observed above the liner via a Laser Doppler Velocimetry (LDV) measurement [78], see Fig. 30. A set of equations (convected Helmholtz [77], linearized Euler [78]) is then chosen and solved numerically. The "numerical" pressure (or velocity) is then compared to its experimental counterpart until convergence is reached. One of the main concerns regarding this strategy is the validity of the obtained impedance value, relative to the presence of different uncertainties. To take into account uncertainties of the measurements or the numerical model, the eduction is recast into a statistical inference problem. Using Bayes' theorem, the posterior probability density of the impedance is obtained, thus representing the information one has on this quantity, after having observed new experimental data [79]. This approach allows taking into account different sources of uncertainties, available prior knowledge, and to yield estimators on the impedance that

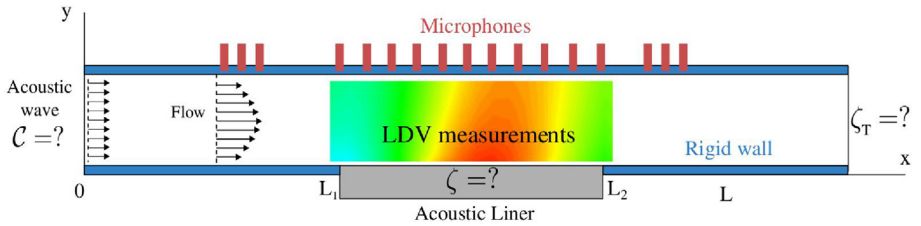

Fig. 30. Schematics of an aero-acoustic bench for liner impedance eduction, showing both the microphone measurement locations and the LDV window.

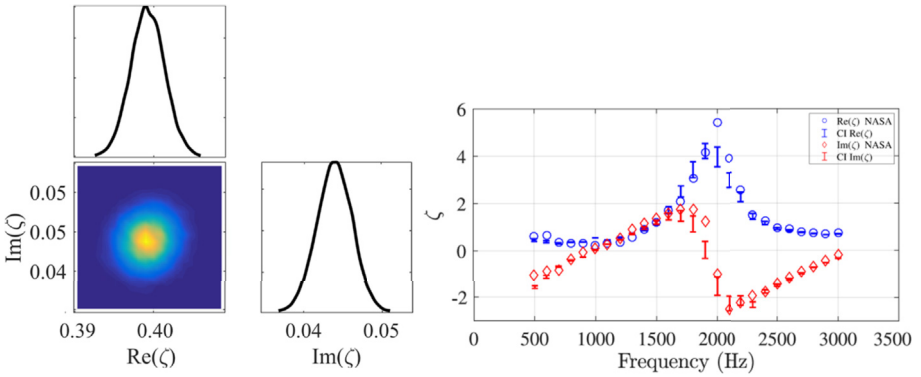

Fig. 31. Left: probability density function of the impedance at f = 1000 Hz and Mach = 0.255. Right: comparison between NASA deterministic eduction method (markers) and Bayesian inference results (error bars), at Mach = 0.255.

are more informative than the single impedance value returned by a classical deterministic approach. The statistical eduction process has been successfully validated on NASA benchmark data (from Ref. [77]). The results are shown in Fig. 31, for material CT57 (ceramic tubular material of 57% porosity), at Mach 0.255.

Written by Rémi Roncen: remi.roncen@onera.fr, *Fabien Méry, Estelle Piot and Frank Simon. ONERA - The French Aerospace Lab, France*

7.8. Fig. of time-domain impedance boundary conditions in aeroacoustics

Improving the reliability of computational aeroacoustics (CAA) is one of the key drivers to achieve noise reduction levels targeted by international regulations. To reduce the noise emitted by an aircraft, one practical solution consists in mounting passive sound absorbing materials, commonly known as acoustical liners. Practical computations of sound absorption are typically done by abstracting the geometrical features of the material using an impedance boundary condition, which in case of time-domain CAA simulations is called a TDIBC. The TDIBC used in the numerical computation must be tailored to the absorbing material considered. [80] has shown that the TDIBC can be derived from a mathematical study of the absorbing material, while being shaped under an expression very close to an improved broadband multipole model. This feature contrasts with the existing purely empirical one-size-fits-all approach (consisting in using a single numerical model postulated a priori), which can lead to computational difficulties for adjusting the fit. The analysis carried out has delivered tailored TDIBCs for a wide range of materials, which covers perforates, semi-infinite ground layers, as well as cavities filled with a porous medium. A computationally-efficient way of performing the time-domain computation has also been laid out in Ref. [81]. It relies on using transport equations and ordinary differential equations and is also a consequence of the mathematical analysis used for tailoring the TDIBC. Moreover, a practical problem encountered in numerical computations is that some materials can impose a stringent reduction in time step, leading to a costly simulation. The analysis presented in Ref. [81] has highlighted a way of cancelling this time step reduction, i.e. of ensuring that the IBC has a neutral impact on the simulation time step (see Fig. 32. This is done using a formulation based

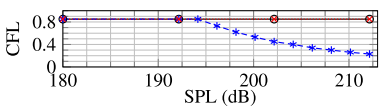

Fig. 32. Maximum allowable Courant–Friedrichs–Lewy (CFL) number against SPL, in an impedance tube configuration. Hard wall (black), non-linear TDIBC with a formulation based on the reflection coefficient (red), non-linear TDIBC with a formulation based on the impedance (blue). The dB levels of the incident wave are arbitrary. (For interpretation of the references to color in this figure legend, the reader is referred to the Web version of this article.)

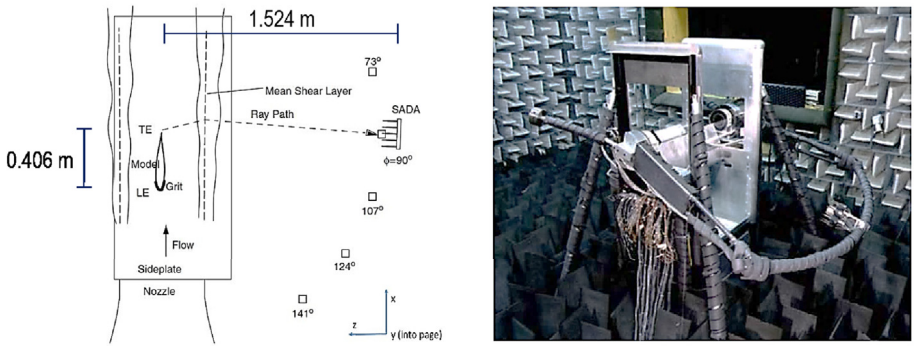

Fig. 33. Setup for the Leading Edge/Trailing Edge measurements of the NACA 63-215 Mod-B full-span airfoil in NASA Langley QFF. The airfoil is installed in a clean configuration at its zero-lift angle of attack (−1.2). The coordinate system origin is the centre of the nozzle exit plane. Credits: Hutcheson and Brooks.

on the reflection coefficient instead of the impedance or admittance.

*Written by E. Piot (*estelle.piot@onera.fr*), F. Monteghetti, ONERA - The French Aerospace Lab, France, D. Matignon, ISAE-Supaero, France.*

7.9. Improved Generalized Inverse Beamforming for airframe noise applications

Thanks to their ability to deal with distributed and coherent acoustic sources, inverse beamforming methods have grown in popularity amongst the aeroacoustic community in the last few decades. An improved version of the Generalized Inverse Beamforming (GIBF) [82] has been developed at von Karman Institute for Fluid Dynamics (VKI) with the objective of ensuring an accurate source localization and a robust source strength reconstruction for airframe noise applications. Specifically, a method based on the Quasi-optimality criterion for the determination of the optimal regularization parameters at each iteration of the algorithm has been implemented. The validation of the technique has been carried out by applying the improved GIBF to an experimental benchmark dataset labelled as NASA2. The test case, Fig. 33 refers to the analysis of a small-scale open-jet facility, the NASA Langley Quiet Flow Facility (QFF), for the characterization of a NACA 63-215 Mod-B full-span airfoil self-noise. The study comprehends the qualitative evaluation of the noise source distribution maps for several one-third octave frequency bands and the quantitative estimation of the integrated one-third octave band spectra of the model leading edge and trailing edge regions. All the maps and the spectra have been compared with the ones obtained with other microphone phased array data processing techniques commonly used in aeroacoustic applications [83]. Results show that, with proper handling of the regularization strategy, GIBF can accurately resolve distributed acoustic noise sources. The sound maps present improvements in terms of readability and reconstruction of the distributed nature of the source, whereas the integrated levels are in close agreement with the ones predicted by the other advanced methods Fig. 34.

Written by R. Zamponi: riccardo.zamponi@vki.ac.be*, von Karman Institute for Fluid Dynamics, Belgium, N. Van de Wyer, von Karman Institute for Fluid Dynamics, Belgium, C. Schram, von Karman Institute for Fluid Dynamics, Belgium*

7.10. Velocity-potential boundary-field integral formulation for sound scattered by moving bodies

A novel boundary-field integral formulation suitable for the prediction of noise scattered by moving bodies has been developed and validated in Ref. [84] in the framework of potential subsonic potential flows. It allows for the appraisal of the role of nonlinear terms in the acoustic scattering computations for those configurations where the nonuniform mean-flow past the scattering body is not negligible. Such an issue is not trivial because it is proven that, starting from the same flow modelling assumptions, linear formulations based on the wave equation for the velocity potential or on the Lighthill equation and the Ffowcs Williams and Hawking's equation for the pressure disturbance, provide different predictions when the scatterer is not at rest. Hence, discrepancies reside in the different influence of the neglected nonlinear terms. The new velocity potential-based approach is developed by extracting the first-order contributions from the nonlinear terms. This yields a linearized boundary-field, frequency-domain formulation for the scattered potential, that extends the standard linear boundary integral approach. The influence of the additional field contributions is examined for different scatterer velocities, with the aim of assessing the domain of validity of the fully linear formulation and the rate of grow of the field contributions with increase of velocity. Specifically, the numerical investigation concerns the noise scattered by a moving, non-lifting wing, when impinged by an acoustic disturbance generated by a co-moving point source.

*Written by M. Gennaretti (*m.gennaretti@uniroma3.it*), G. Bernardini, C. Poggi, Roma Tre University, Italy and C. Testa CNR-INM, Italy.*

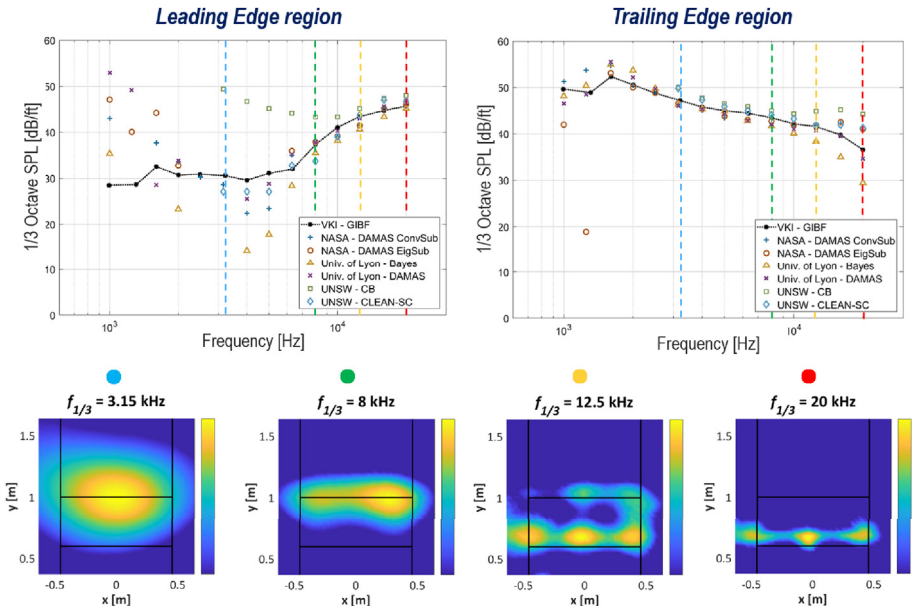

Fig. 34. Integrated leading edge and trailing edge one-third octave band spectra per-foot-span computed with various microphone phased array data processing techniques and GIBF noise source distribution maps referred to different one-third octave band frequencies. Credits: Christopher Bahr.

7.11. Aerodynamic noise of large-scale vortex ring produced by explosion

Aeroacoustic properties of large-scale turbulent vortex rings produced by means of an explosion in steel cylindrical chambers (Fig. 35) are considered [85]. Unlike the small-scale experiments in which the noise of the ring is determined by spectra averaging over an ensemble of similar realizations, in the case of large-scale rings generated by the explosion it is possible to investigate the phenomenon on the basis of only a single realization. It significantly extends the range of parameters that can be analyzed. The large-scale ring noise manifests itself by strong peaking of the spectrum in a narrow frequency band as well as the small-scale one (Fig. 36). However one could recognize two or even three narrow frequency bands which are close to the

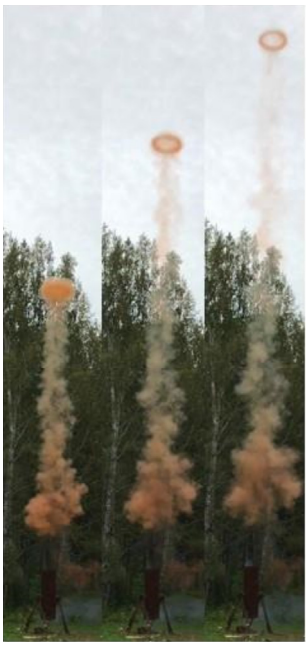

Fig. 35. High speed camera diagnostics of vertical movement of the vortex ring, duct diameter 80 cm.

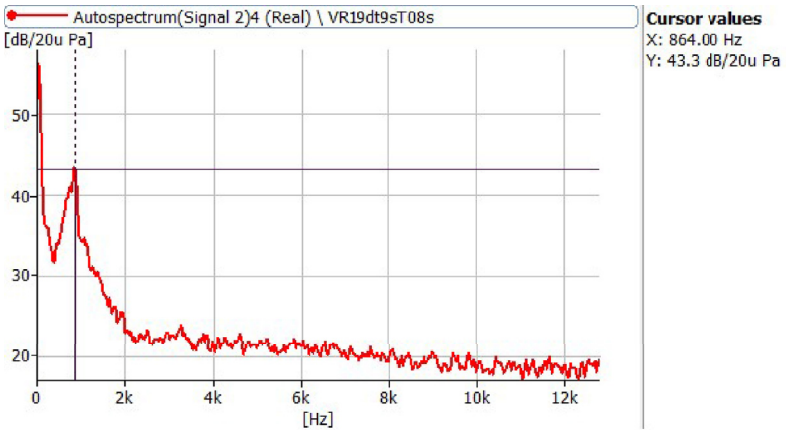

Fig. 36. Narrow band spectra for the vortex ring with time delay after explosion 10 s, duct 80 cm.

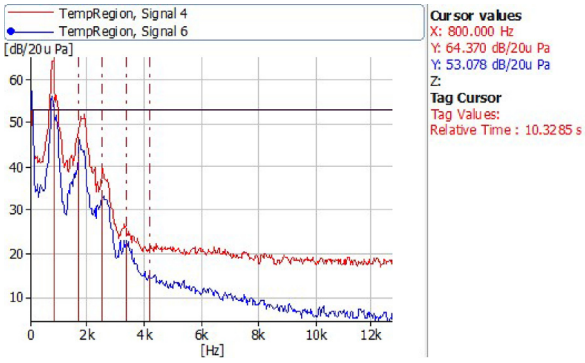

Fig. 37. Multi-peaking structure of vortex ring noise for different conditions. Vortex ring moves along the ground surface, measurements produced by two different mics located at different distances from the trajectory (different colors). (For interpretation of the references to color in this figure legend, the reader is referred to the Web version of this article.)

multiple frequencies of the main peak (Fig. 37), but the amplitudes of these peaks are significantly lower. The main frequency peak does not shift to a lower-frequency region while the ring moves. It fundamentally differs from the case of the small-scale rings, which in turn is in agreement with the self-similar theory of the vortex ring motion [86]. This difference means that the vortex core behaviour of such vortices has some peculiarities, although the presence of several peaks is consistent with the results of the theory of vortex ring sound generation [87].

*Written by V.F.Kopiev: (*vkopiev@mktsagi.ru*), TsAGI, Russian Federation.*

8. Miscellaneous topics

8.1. Vehicle cabin noise

An important part of the noise inside vehicle cabins is emitted from window vibration. The vibration is excited both hydrodynamically (due to exterior flow impingement on windows) and acoustically (due to exterior flow-induced noise). The flows induced by side-view mirrors upstream of the windows can significantly contribute to the excitation. As a simplification of a mirror, a hemisphere embedded in a free stream was investigated using large eddy simulation (LES) [88]. The wake was found to contain predominant exterior noise sources. Furthermore, wake impingement was explored by placing a quarter-spherocylinder blunt body (termed the generic side-view mirror) on a plate (Fig. 38) in a study on cavity interior noise using LES coupled with a finite element method [89]. The analysis of wavenumber-frequency spectra addressed the inhomogeneous feature of surface pressure fluctuations, of which the hydrodynamic component has bent spectral energy ridges due to the inhomogeneous mean convection. The flow inhomogeneity, however, has less influence on the noise magnitude distribution at natural frequencies, as compared to the mode shapes of the window and cavity (Fig. 39). In addition, the efficiencies of the hydrodynamic and acoustic components in the interior noise generation were quantified. Since the quality of cabin noise prediction is dependent on the accuracy of the inputs to the prediction (surface pressure fluctuations), a study on CFD methods for exterior flows and noise was motivated regarding compressibility, turbulence modelling including improved delayed detached eddy simulation (IDDES) and

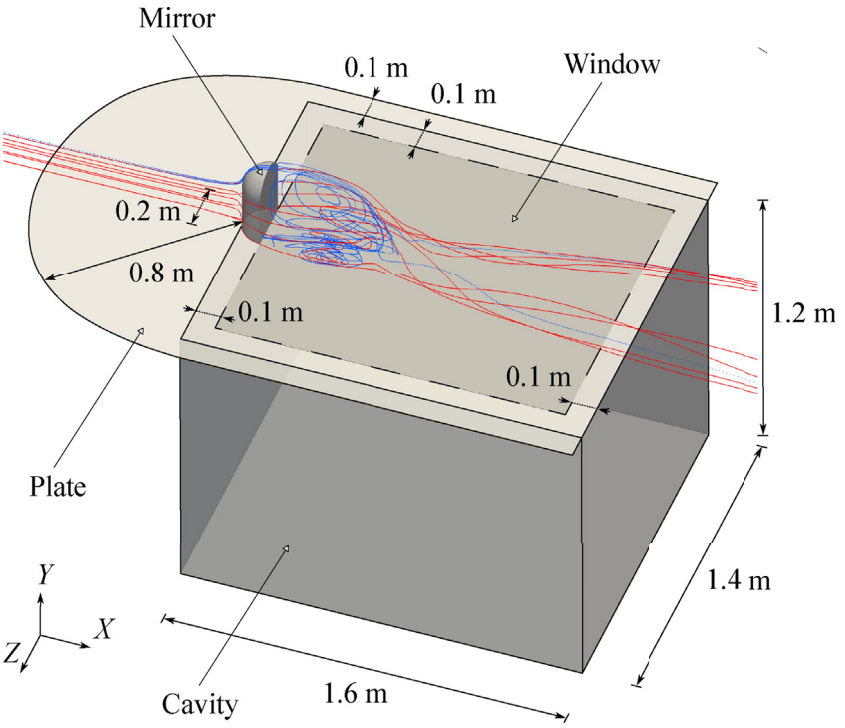

Fig. 38. The configuration with streamlines of the time-averaged velocity. The streamlines past the mirror upper edge are colored in blue, and those past the side edges colored in red. (For interpretation of the references to color in this figure legend, the reader is referred to the Web version of this article.)

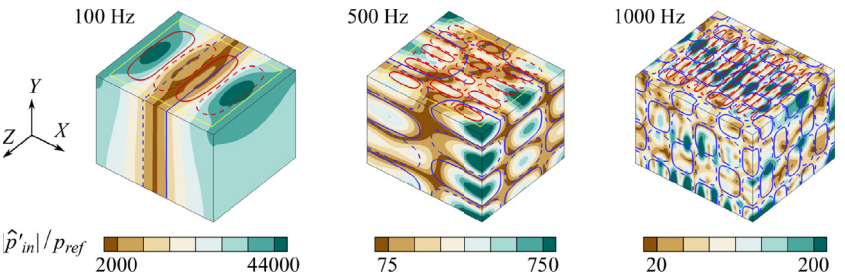

Fig. 39. Contours of the interior noise magnitudes at 100 Hz, 500 Hz, and 1000 Hz. From left to right, the red lines show the window mode shapes at 101.6 Hz, 503 Hz, and 998 Hz the blue lines show the cavity mode shapes at 106.3 Hz, 501.5 Hz, and 1000.4 Hz. The solid and dashed line patterns represent the normalized mode shape levels of 0.1 and −0.1, respectively. (For interpretation of the references to color in this figure legend, the reader is referred to the Web version of this article.)

LES, and grid topology [90]. The compressible IDDES was down-selected based on its comparatively better performance. This method was then applied to simulate real truck side-view mirrors, which are mounted on a simplified truck body [91]. It was identified that intensive surface pressure fluctuations on the window are mainly caused by the impingement of the free shear layers that initiate from the mirrors and A-pillar.

Written by H.-D. Yao: huadong.yao@chalmers.se*, and L. Davidson, Department of Mechanics and Maritime Sciences, Chalmers University of Technology, Sweden.*

8.2. Assessing the stochastic error of in-duct multi-microphone measurements

In-duct multi-microphone measurements are used to determine the acoustic properties of components such as acoustic liners. This can involve wave decomposition and determination of scattering matrices. To be able to compare measured results with model predictions, the quality of the measurements have to be known. Uncertainty analyses are invaluable to assess and improve the quality of measurement results in terms of accuracy and precision. Linear analyses are widespread, computationally fast and give information of the contribution of each error source to the overall measurement uncertainty, however, they can not be applied in every situation. The purpose of the study presented in this highlight [92], was to determine if linear methods

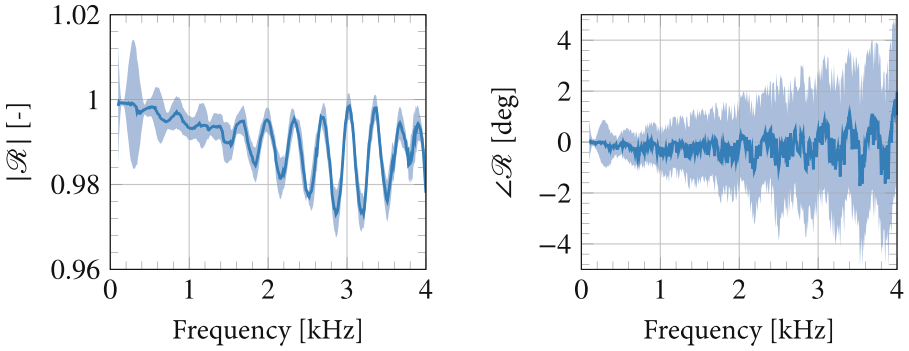

Fig. 40. Measured reflection coefficient of a rigid wall with 95% confidence interval. Left absolute value, right phase.

can be used to assess the quality of acoustic scattering matrices. A linear uncertainty analysis was applied to acoustic scattering matrix measurements and the results were compared against Monte-Carlo simulations. It was shown that a linear uncertainty analysis, applied to the wave decomposition method, gives correct results for plane waves when three conditions are satisfied. An example of a result, including a 95% confidence interval, for the reflection coefficient of a rigid wall duct termination, can be seen in Fig. 40. When higher order modes are present, the number of conditions that have to be simultaneously satisfied increases with the number of cut-on higher order modes and it is better to resort to a different method. The method was based on matrix perturbation theory and gives qualitative information in the form of partial condition numbers and the implementation is straightforward. Using the alternative method, the measurements of higher order modes were analyzed and the observed difference in the measured reflection coefficients for different excitation conditions was explained by the disparity in modal amplitude.

Written by Hans Bodén: hansbod@kth.se, *KTH, Sweden*

8.3. Nonlinear asymptotic impedance model for a Helmholtz resonator of finite depth

In order to model the impedance of an acoustic liner composed of an array of Helmholtz resonators, a weakly nonlinear theory is developed for the resonance regime of a finite-length Helmholtz resonator, based on the acoustics of an organ pipe connected to the external excitation field via an acoustically small neck. The flow through the neck includes linear viscous friction and nonlinear dissipation due to flow separation and vortex shedding. Recent work upon which this highlight is based [93], extends and refines the previous analysis [94], which considered an acoustically compact cavity.

The weakly nonlinear model allows a solution, asymptotic for small, but also moderate, excitation amplitudes. This enables analytically obtaining an expression for the impedance that includes nonlinear effects for frequencies close to the fundamental resonance frequency.

Considering the small number of modelling assumptions, the obtained results compare very well with experimental data by Motsinger & Kraft [95] in the linear and nonlinear impedance regimes. See Fig. 41

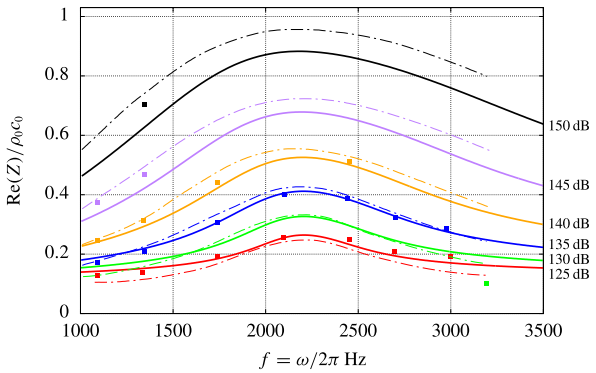

Fig. 41. Comparison of impedance resistance $\Re(Z)/\rho_0 c_0$, as given by new theory (solid lines), with measurements (squares) and predictions (dash-dotted lines) by Motsinger & Kraft in Ref. [95].

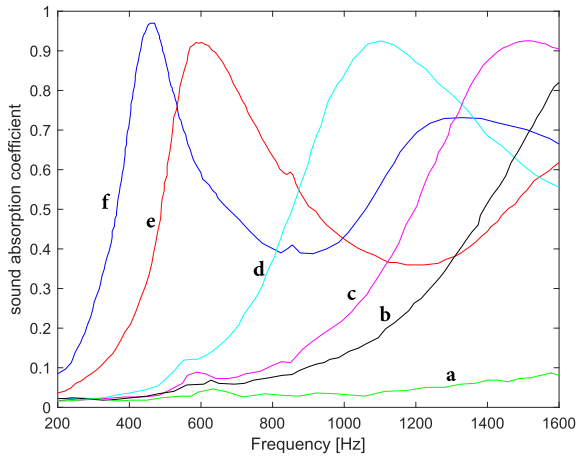

Fig. 42. Sound absorption coefficient as a function of frequency for various β disk piles. Curves a, b, c, d, e and f refer, respectively, to samples β1, β1-4, β1-6, β1-10, β1-17 and β1-22, (βi-j means the pile made of all disks from the i-th to j-th.

Written by Sjoerd W. Rienstra: s.w.rienstra@tue.nl*, TUE, The Netherlands and Deepesh Kumar Singh, TUE, The Netherlands, (now: Lilium, Germany)*

8.4. Analytical prediction of limit-cycle oscillations amplitude in solid rocket motors

In large Solid Rocket Motors (SRMs), vortex-driven indirect sound leads to the establishment of a feedback loop resulting in self-sustained limit-cycle pressure pulsations [96–98]. Paramount to this mechanism is the interaction of vortices, created near a geometric feature of the combustion chamber, with the nozzle as they exit [99]. For vortex-driven self-sustained pressure pulsations, the presence of a cavity around the choked nozzle inlet has been demonstrated to have a major influence. Indeed, cold-gas experiments of a scale model of the Ariane 5 SRM have shown that the limit-cycle amplitude of vortex- driven self-sustained pressure pulsations are proportional to the nozzle cavity volume [96]. Hirschberg et al. [99] have used dedicated vortex-nozzle interaction simulations, based on a frictionless compressible model proposed by Hulshoff et al. [100], to develop a new scaling law for this indirect sound source. Hirschberg et al. identified key parameters, viz., the nozzle inlet Mach number, the vortex circulation and the dynamic pressure upstream from the nozzle [99]. Using an energy balance approach, Hirschberg et al. [98] formulated an analytical model which predicts, within an order of magnitude, pulsation amplitudes observed in cold gas-scale experiments of Ariane 5. Both this analytical model and the numerical study of vortex-nozzle interaction confirmed the importance of the nozzle cavity volume.

Written by Lionel Hirschberg: l.hirschberg@me.com*, von Karman Institute for Fluid Dynamics, Belgium and Centrale Supélec, France*

8.5. Light electrospun polyvinylpyrrolidone blankets

Traditional sound absorption materials (foams, fibres, membranes, etc.,) have good noise reduction abilities at high-frequency, but exhibit insufficient sound absorption properties in the low and medium frequency range in which human sensitivity to noise is fairly high. Therefore, materials with excellent noise reduction properties in the low and medium frequency range are highly desirable for acoustical purposes. Polymeric soundproofing materials have been fabricated by electrospinning polyvinylpyrrolidone (PVP) [101]. The mats were produced in the form of thin disks of 10 cm in diameter with a fibre diameter of (1.6 ± 0.5) or (2.8 ± 0.5) μm. The sound absorption coefficients were measured using an impedance tube instrument. For a given set of disks (from a minimum of 6) the sound absorption coefficient changed with the frequency (in the range 200–1600 Hz) following a bell shape curve with a maximum (where the coefficient is greater than 0.9) that shifts to lower frequencies with an increasing number of piled disks and with greater fibre diameter (Fig. 42). The acoustic behaviour can be continuously tuned by changing the mass of the blanket (number of plies).

Moreover, in order to improve flame retardancy that often, because of very severe regulations (as in aerospace engineering), prevents the applicability of materials, the addition of graphene in the PVP blanket has been considered [101,102] and the sound absorption coefficient has been evaluated for different concentrations [103]. Results reported in Fig. 43 for a PVP blanket (mass of about 7.5 ± 0.5 g), reveal that the addition of graphene does not lower the very high sound absorption coefficient value but it affects, in a non-monotonous manner, the bell-shaped curves versus frequency becoming sharper and moving to higher frequency at the lower graphene addition. The opposite is observed when the graphene content is further increased.

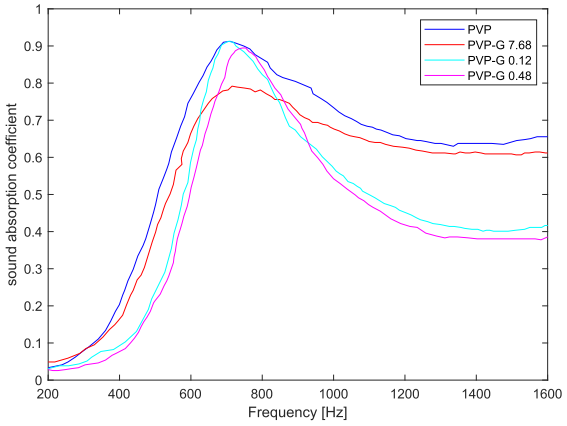

Fig. 43. Comparison of sound absorption coefficient as a function of frequency of PVP blankets without and with the addition of graphene of different concentrations.

Written by Giuseppe Petrone (giuseppe.petrone@unina.it), Francesco Marulo, Francesco Branda, University of Naples Federico II, Italy

References

[1] S. Pron, T. Renaud, M. Terracol, C. Benoit, I. Mary, An immersed boundary method for preliminary design aerodynamic studies of complex configurations, in: 23rd AIAA Computational Fluid Dynamics Conference, AIAA, 2017, p. 3623.
[2] S. Redonnet, S. Ben Khelil, J. Bult, G. Cunha, Numerical characterization of landing gear aeroacoustics using advanced simulation and analysis techniques, J. Sound Vib. 403 (2017) 214–233.
[3] D.C. Mincu, T. Le Garrec, S. Peron, M. Terracol, Immersed boundary conditions for high order caa solvers-aeroacoustics installation effects assessment, in: 23rd AIAA/CEAS Aeroacoustics Conference, AIAA, 2017, p. 3504.
[4] J. Wickerhoff, T. Sijpkes, Aeroplane provided with Noise-Reducing Means, as Well as a Landing Gear and Blowing Means, 2004.
[5] S. Oerlemans, A. de Bruin, Reduction of landing gear noise using an air curtain, in: 15th AIAA/CEAS Aeroacoustics Conference (30th AIAA Aeroacoustics Conference), American Institute of Aeronautics and Astronautics, Miami, Florida, 2009.
[6] K. Zhao, X.-x. Yang, P.N. Okolo, W.-h. Zhang, Gareth J. Bennett, Use of a plane jet for flow-induced noise reduction of tandem rods, Chin. Phys. B 25 (2016) 064301-1–064301-9.
[7] Kun Zhao, Patrick N. Okolo, John Kennedy, Gareth J. Bennett, A study of planar jet flow control and perforated fairings for the reduction of the flow-induced noise of tandem rods in a cross-flow (AIAA2016-2772), in: 22nd AIAA/CEAS Aeroacoustics Conference, AIAA, Lyon, France, 2016.
[8] K. Zhao, S. Alimohammadi, P.N. Okolo, J. Kennedy, G.J. Bennett, Aerodynamic noise reduction using dual-jet planar air curtains, J. Sound Vib. 432 (2018) 192–212.
[9] K. Zhao, X. Yang, P.N. Okolo, Z. Wu, G.J. Bennett, Use of dual planar jets for the reduction of flow-induced noise, AIP Adv. 7 (2017) 025312-1–025312-7.
[10] K. Zhao, P.N. Okolo, Y. Wang, J. Kennedy, G.J. Bennett, An experimental characterization of the interaction between two tandem planar jets in a crossflow, J. Fluids Eng. 140 (2018) 111106-1–111106-12.
[11] K. Zhao, P.N. Okolo, J. Kennedy, G.J. Bennett, 2D PIV measurement on the interaction zone between two parallel planar jets in a crossflow, AIP Adv. 7 (2017) 105104-1–105104-21.
[12] K. Zhao, X. Yang, P.N. Okolo, Z. Wu, W. Zhang, G.J. Bennett, A novel method for defining the Leeward edge of the planar jet in crossflow, J. Appl. Fluid Mech. 10 (2017) 1475–1486.
[13] Gareth J. Bennett, Patrick N. Okolo, Kun Zhao, John Philo, Yaoyi Guan, Scott C. Morris, Cavity resonance suppression using fluidic spoilers, AIAA J. 57 (2018) 706–719.
[14] Eleonora Neri, John Kennedy, Massimiliano Di Giulio, Ciaran O'Reilly, Jeremy Dahan, Marco Esposito, Massimiliano Bruno, Francesco Amoroso, Antonello Bianco, Gareth J. Bennett, Characterization of low noise technologies applied to a full scale fuselage mounted nose landing gear, in: Internoise2015: Proceedings of the Internoise 2015/ASME NCAD Meeting, American Society of Mechanical Engineers, 2015, Paper No: NCAD20155911.
[15] Eleonora Neri, John Kennedy, Gareth J. Bennett, Aeroacoustic source separation on a full scale nose landing gear featuring combinations of low noise technologies, in: Internoise2015: Proceedings of the Internoise 2015/ASME NCAD Meeting, American Society of Mechanical Engineers, San Francisco, CA, USA, 2015, Paper No: NCAD20155912.
[16] Petr Eret, John Kennedy, Gareth J. Bennett, Effect of noise reducing components on nose landing gear stability for a mid-size aircraft coupled with vortex shedding and freeplay, J. Sound Vib. 354 (2015) 91–103.
[17] Gareth J. Bennett, Eleonora Neri, John Kennedy, Noise characterization of a full-scale nose landing gear, J. Aircr. 55 (2018) 2476–2490.
[18] Eleonora Neri, John Kennedy, Gareth J. Bennett, Bay cavity noise for full-scale nose landing gear: a comparison between experimental and numerical results, Aero. Sci. Technol. 72 (2018) 278–291.
[19] Gareth J. Bennett, David B. Stephens, Francisco Rodriguez Verdugo, Resonant mode characterisation of a cylindrical Helmholtz cavity excited by a shear layer, J. Acoust. Soc. Am. 141 (2017) 7–18.
[20] Roberto Merino Martinez, Eleonora Neri, Mirjam Snellen, John Kennedy, Dick Simons, Gareth J. Bennett, Analysis of nose landing gear noise comparing numerical computations, prediction models and flyover and wind-tunnel measurements, in: 24th AIAA/CEAS Aeroacoustics Conference, 2018-3299, American Institute of Aeronautics and Astronautics, Georgia, Atlanta, USA, 2018.
[21] John Kennedy, Elenora Neri, Gareth J. Bennett, The reduction of main landing gear noise, in: 22nd AIAA/CEAS Aeroacoustics Conference, Lyon, France, AIAA, 2016, p. 2900.
[22] Saloua Ben Khelil, Philippe Bardoux, Jean-Luc Godard, Thomas Le Garrec, John Kennedy, Gareth J. Bennett, Investigation of the noise emission of a regional aircraft main landing gear bay, in: 23rd AIAA/CEAS Aeroacoustics Conference, American Institute of Aeronautics and Astronautics, Denver, Colorado, USA, 2017.
[23] S.R. Koh, B. Zhou, M. Meinke, N. Gauger, W. Schrder, Numerical analysis of the impact of variable porosity on trailing-edge noise, Comput. Fluids 167 (2018) 66–81.

[24] S.R. Koh, M. Meinke, W. Schrder, Numerical analysis of the impact of permeability on trailing-edge noise, J. Sound Vib. 421 (2018) 348–376.
[25] C. Kucukosman, J. Christophe, C.F. Schram, Rans-based trailing-edge noise prediction using Amiet's theory: accuracy and mesh sensitivity of semi-empirical and integral wall pressure models, in: AIAA, 2018, p. 3793.
[26] R. Amiet, Noise due to turbulent flow past a trailing edge, J. Sound Vib. 47 (1976) 387–393.
[27] R.L. Panton, J.H. Linebarger, Wall pressure spectra calculations for equilibrium boundary layers, J. Fluid Mech. 65 (1974) 261.
[28] S. Lee, Empirical wall-pressure spectral modeling for zero and adverse pressure gradient flows, AIAA J. 56 (2018) 1818–1829.
[29] D.-Y. Maa, Potential of microperforated panel absorbers, J. Acoust. Soc. Am. 104 (1998) 2861–2866.
[30] C. Maury, T. Bravo, D. Mazzoni, The use of microperforations to attenuate the cavity pressure fluctuations induced by a low-speed flow, J. Sound Vib. 439 (2019) 1–16.
[31] F. Avallone, W. Van Der Velden, D. Ragni, D. Casalino, Noise reduction mechanisms of sawtooth and combed-sawtooth trailing-edge serrations, J. Fluid Mech. 848 (2018).
[32] D. Ragni, F. Avallone, W. van der Velden, D. Casalino, Measurements of near-wall pressure fluctuations for trailing-edge serrations and slits, Exp. Fluid 60 (2019) 6.
[33] D. Casalino, F. Avallone, I. Gonzalez-Martino, D. Ragni, Aeroacoustic study of a wavy stator leading edge in a realistic fan/OGV stage, J. Sound Vib. 442 (2019) 138–154.
[34] F. Avallone, D. Casalino, D. Ragni, Impingement of a propeller-slipstream on a leading edge with a flow-permeable insert: a computational aeroacoustic study, Int. J. Aeroacoustics 17 (2018) 687–711.
[35] A. Rubio Carpio, R. Merino-Martnez, F. Avallone, D. Ragni, M. Snellen, S. van der Zwaag, Experimental characterization of the turbulent boundary layer over a porous trailing edge for noise abatement, J. Sound Vib. 443 (2019) 537–558.
[36] M. Daroukh, C. Polacsek, A. Chelius, Shockwave generation and radiation from an UHBR engine with flow distortion using a CFD/CAA chaining strategy, in: 25th AIAA/CEAS Aeroacoustics Conference, American Institute of Aeronautics and Astronautics, 2019(AIAA 2019-2605).
[37] L. Cambier, S. Heib, S. Plot, The Onera elsA CFD software: input from research and feedback from industry, Mech. Ind. 14 (2013) 159–174.
[38] J. Thisse, C. Polacsek, J. Mayeur, S. Khelladi, X. Gloerfelt, A. Lafitte, Numerical simulations of shock-wave propagation in turbofan intakes, in: In 22nd AIAA/CEAS Aeroacoustics Conference, AIAA, 2016, p. 2879.
[39] A. Pereira, J. Regnard, E. Salze, F. Gea-Aguilera, M. Gruber, New modular fan rig for advanced aeroacoustic tests - modal decomposition on a 20 UHBR fan stage, in: Proceedings of the 25th AIAA/CEAS Aeroacoustics Conference, Delft, Netherlands, AIAA, 2019, p. 2604.
[40] C. Brandstetter, B. Paoletti, X. Ottavy, Compressible modal instability onset in an aerodynamically mistuned transonic fan, J. Turbomach. 141 (2019) 031004.
[41] Q. Leclre, A. Pereira, C. Bailly, J. Antoni, C. Picard, A unified formalism for acoustic imaging based on microphone array measurements, Int. J. Aeroacoustics 16 (2017) 431–456.
[42] M. Shur, M. Strelets, A. Travin, J. Christophe, K. Kucukcoskun, C.F. Schram, S. Sack, M. Abom, Effect of inlet distortions on ducted fan noise, in: Proceedings of the 22nd AIAA/CEAS Aeroacoustics Conference, 2016.
[43] R.J. Dominique, J. Christophe, C. Schram, Multi-port eduction of installation effects applied to a small axial fan, Acta Acustica United Acustica 105 (2019) 75–85.
[44] J. Lavrentjev, M. Abom, Characterization of fluid machines as acoustic multi-port sources, J. Sound Vib. 197 (1996) 1–16.
[45] J.C. Tyacke, Z.-N. Wang, P.G. Tucker, LES-RANS of installed ultra-high-bypass-ratio coaxial jet aeroacoustics with flight stream, AIAA J. 57 (2019) 1215–1236.
[46] Z.-N. Wang, J. Tyacke, P. Tucker, P. Boehning, Parallel computation of aeroacoustics of industrially relevant complex-geometry aeroengine jets, Comput. Fluids 178 (2019) 166–178.
[47] J.C. Tyacke, Z.-N. Wang, P.G. Tucker, Noise source, length and time scale distributions in installed jets with a flight stream, in: 2018 AIAA/CEAS Aeroacoustics Conference, 2018, p. 3619.
[48] S. Modini, G. Graziani, G. Bernardini, M. Gennaretti, Pressure feedback-based bladevortex interaction noise controller for helicopter rotors, Int. J. Aeroacoustics 17 (2018) 295–318.
[49] S. Modini, G. Graziani, G. Bernardini, M. Gennaretti, Blade-vortex interaction noise controller based on miniature trailing edge effectors, Int. J. Acoust. Vib. 23 (2018).
[50] M. Gennaretti, G. Bernardini, J. Serafini, G. Romani, Rotorcraft comprehensive code assessment for bladevortex interaction conditions, Aero. Sci. Technol. 80 (2018) 232–246.
[51] G. Bernardini, J. Serafini, M.M. Colella, M. Gennaretti, Analysis of a structural-aerodynamic fully-coupled formulation for aeroelastic response of rotorcraft, Aero. Sci. Technol. 29 (2013) 175–184.
[52] A.V. Smolyakov, V.M. Tkachenko, Models of a field of pseudosound turbulent wall pressures and experimental data, Akust. Zh. 37 (1991) 1199–1207.
[53] A. Klabes, Aircraft Fuselage Vibration Excitation by Turbulent Boundary Layer Flow in Cruise, Ph.D. thesis, Institute of Aerodynamics and Flow Technology, German Aerospace Center, 2017.
[54] N. Hu, S. Callsen, A parametric study on wall pressure wavenumber-spectrum models with application to aircraft fuselage vibration prediction, in: 26th International Congress on Sound and Vibration, 2019.
[55] Gareth J. Bennett, John Kennedy, Petr Eret, Filippo Cappadona, Antonello Bianco, Raffaele Letizia, Davide Danise, Lucille Lamotte, Christophe Picard, Arthur Finez, Paolo Castellini, Paolo Chiariotti, Francesca Sopranzetti, Demosthenis Tsahalis, Haralabos Tsahalis, Vassilios Moussas, Antonio Paonessa, Francesco Amoroso, Massimiliano Di Giulio, WENEMOR: wind tunnel tests for the evaluation of the installation effects of noise emissions of an open rotor advanced regional aircraft (AIAA 2013-2092), in: 19th AIAA/CEAS Aeroacoustics Conference (32nd AIAA Aeroacoustics Conference), American Institute of Aeronautics and Astronautics, Berlin, Germany, 2013.
[56] John Kennedy, Petr Eret, Gareth J. Bennett, Paolo Castellini, Paolo Chiariotti, Francesca Sopranzetti, Christophe Picard, Arthur Finez, The application of advanced beamforming techniques for the noise characterization of installed counter rotating open rotors (AIAA 2013-2093), in: 19th AIAA/CEAS Aeroacoustics Conference (32nd AIAA Aeroacoustics Conference), American Institute of Aeronautics and Astronautics, Berlin, Germany, 2013.
[57] John Kennedy, Petr Eret, Gareth J. Bennett, A parametric study of installed counter rotating open rotors, in: 19th AIAA/CEAS Aeroacoustics Conference (32nd AIAA Aeroacoustics Conference), American Institute of Aeronautics and Astronautics, Berlin, Germany, 2013 (AIAA 2013-2094).
[58] J. Kennedy, P. Eret, Gareth J. Bennett, A parametric study of airframe effects on the noise emission from installed contra-rotating open rotors, Int. J. Aeroacoustics 17 (2018) 624–654.
[59] P. Eret, J. Kennedy, F. Amoroso, P. Castellini, Gareth J. Bennett, Experimental observations of an installed-on-pylon contra-rotating open rotor with equal blade number in pusher and tractor configuration, Int. J. Aeroacoustics 15 (2016) 228–249.
[60] L. Sanders, D.-C. Mincu, Pl Vitagliano, M. Minervino, J. Kennedy, G. Bennett, Prediction of the acoustic shielding by aircraft empennage for contra-rotating open rotors, Int. J. Aeroacoustics 16 (2017) 626–648.
[61] Laurent Sanders, Daniel C. Mincu, Williams Denis, Pier Luigi Vitagliano, Mauro Minervino, John Kennedy, Petr Eret, Gareth J. Bennett, A coupling of computational methods for CROR installation effects (AIAA 2014-3190), in: AIAA Aviation, 20th AIAA/CEAS Aeroacoustics Conference, American Institute of Aeronautics and Astronautics, Atlanta, GA, USA, 2014.
[62] C. Horvth, B. Fenyvesi, B. Kocsis, M. Quaglia, S. Moreau, J. Kennedy, G.J. Bennett, Towards counter-rotating open rotor noise reduction via radiation efficiency considerations, in: 25th AIAA/CEAS Aeroacoustics Conference, American Institute of Aeronautics and Astronautics, Delft, The Netherlands, 2019.
[63] V.F. Kopiev, S.A. Chernyshev, Methods of the Lagrangian and Hamiltonian mechanics in aeroacoustics problems, Acoust Phys. 64 (2018) 707–717.
[64] O. Jiek, Aeroacoustics research in Europe: the CEAS-ASC report on 2015 highlights, J. Sound Vib. 381 (2016) 101–120.
[65] V. Fleury, R. Davy, Analysis of jetairfoil interaction noise sources by using a microphone array technique, J. Sound Vib. 364 (2016) 44–66.

[66] T. Brooks, W. Humphreys, A deconvolution approach for the mapping of acoustic sources (damas) determined from phased microphone arrays, J. Sound Vib. 294 (2006) 856–879.
[67] F. Mortain, F. Clro, D. Palmieri, Full scale acoustic source identification on VEGA launch pad at lift-off, in: 26th International Congress on Sound and Vibration, 2019.
[68] S. Fauqueux, R. Davy, Modal deconvolution method in a finite circular duct, using flush-mounted microphones, in: 24th AIAA/CEAS Aeroacoustics Conference, 2018-3927, AIAA, Atlanta, Georgia, 2018.
[69] M. Laban, J. Kok, H. Brouwer, CFD/CAA analysis of UHBR engine tonal noise, in: 24th AIAA/CEAS Aeroacoustics Conference, 2018-3780, AIAA, Atlanta, Georgia, 2018.
[70] T. Kuhn, J. Durrwachter, F. Meyer, A. Beck, C. Rohde, C.-D. Munz, Uncertainty quantification for direct aeroacoustic simulations of cavity flows, J. Theor. Comput. Acoustics 27 (2019) 1850044.
[71] M. Moessner, C.A. Kissner, J. Delfs, L. Enghardt, Computational chain for virtual fly-over simulations applied to fan noise, in: 2018 AIAA/CEAS Aeroacoustics Conference, 2018-3782, American Institute of Aeronautics and Astronautics, Atlanta, Georgia, 2018.
[72] C. Kissner, S. Gurin, L. Enghardt, H. Siller, M. Pott-Pollenske, The challenge of tonal fan noise prediction for an aircraft engine in flight, Acta Acustica United Acustica 105 (2019) 17–29.
[73] S. Luesutthiviboon, A.M. Malgoezar, R. Merino-Martinez, M. Snellen, P. Sijtsma, D.G. Simons, Enhanced HR-CLEAN-SC for resolving multiple closely spaced sound sources, Int. J. Aeroacoustics 18 (2019) 392–413.
[74] P. Sijtsma, CLEAN based on spatial source coherence, Int. J. Aeroacoustics 6 (2007) 357–374.
[75] P. Sijtsma, R. Merino-Martinez, A.M.N. Malgoezar, M. Snellen, Highresolution CLEANSC: theory and experimental validation, Int. J. Aeroacoustics 16 (2017) 274–298.
[76] R. Merino-Martinez, E. Neri, M. Snellen, J. Kennedy, D. Simons, G. Bennett, Analysis of nose landing gear noise comparing numerical computations, prediction models and flyover and windtunnel measurements, in: 24th AIAA/CEAS Aeroacoustics Conference, AIAA, Atlanta, Georgia, USA, 2018, June 2529 paper 20183299.
[77] M.G. Jones, W.R. Watson, T.L. Parrott, Benchmark data for evaluation of aeroacoustic propagation codes with grazing flow, in: AIAA, 2005, paper 2853 (2005).
[78] J. Primus, E. Piot, F. Simon, An adjoint-based method for liner impedance eduction: validation and numerical investigation, J. Sound Vib. 332 (2013) 58–75.
[79] R. Roncen, F. Mry, E. Piot, F. Simon, Statistical inference method for liner impedance eduction with a shear grazing flow, AIAA J. 57 (2019) 1055–1065.
[80] F. Monteghetti, D. Matignon, E. Piot, L. Pascal, Design of broadband time-domain impedance boundary conditions using the oscillatory-diffusive representation of acoustical models, J. Acoust. Soc. Am. 140 (2016) 1663–1674.
[81] F. Monteghetti, D. Matignon, E. Piot, Energy analysis and discretization of nonlinear impedance boundary conditions for the time-domain linearized euler equations, J. Comput. Phys. 375 (2018) 393–426.
[82] T. Suzuki, L1 generalized inverse beam-forming algorithm resolving coherent/incoherent, distributed and multipole sources, J. Sound Vib. 330 (2011) 5835–5851.
[83] C.J. Bahr, W.M. Humphreys, D. Ernst, T. Ahlefeldt, C. Spehr, A. Pereira, Q. Leclre, C. Picard, R. Porteous, D. Moreau, J.R. Fischer, C.J. Doolan, A comparison of microphone phased array methods applied to the study of airframe noise in wind tunnel testing, in: 23rd AIAA/CEAS Aeroacoustics Conference, American Institute of Aeronautics and Astronautics, Denver, Colorado, 2017.
[84] M. Gennaretti, G. Bernardini, C. Poggi, C. Testa, Velocity-potential boundary-field integral formulation for sound scattered by moving bodies, AIAA J. 56 (2018) 3547–3557.
[85] Kopiev, M., Zaytsev, V., Akhmetov, D., Nikulin, V., Aerodynamic noise generated by large-scale vortex ring. In: 25th International Congress of Sound and Vibration (ICSV 25).
[86] D.G. Achmetov, Vortex Rings, Springer, Berlin, 2009. OCLC: 492248946.
[87] V.F. Kopiev, S.A. Chernyshev, Vortex ring eigen-oscillations as a source of sound, J. Fluid Mech. 341 (1997) 19–57.
[88] H.-D. Yao, L. Davidson, Noise radiated by low-Reynolds number flows past a hemisphere at Ma0.3, Phys. Fluids 29 (7) (2017) 076102.
[89] H.-D. Yao, L. Davidson, Generation of interior cavity noise due to window vibration excited by turbulent flows past a generic side-view mirror, Phys. Fluids 30 (2018) 036104.
[90] H.-D. Yao, L. Davidson, Z. Chroner, Investigation of Interior Noise from Generic Side-View Mirror Using Incompressible and Compressible Solvers of DES and LES, SAE Technical Paper, 2018. 2018010735.
[91] H.-D. Yao, L. Davidson, Z. Chroner, Simplifications Applied for Simulation of Turbulence Induced by a Side View Mirror of a Full-Scale Truck Using DES, SAE Technical Paper, 2018. 2018010708.
[92] L. Peerlings, F. Bake, S. Boij, H. Bodn, Assessing the stochastic error of acoustic scattering matrices using linear methods, Int. J. Spray Combust. Dyn. 10 (2018) 380–392.
[93] S.W. Rienstra, D.K. Singh, Nonlinear asymptotic impedance model for a Helmholtz resonator of finite depth, AIAA J. 56 (2018) 1792–1802.
[94] Sjoerd W. Rienstra, Deepesh Kumar Singh, Nonlinear asymptotic impedance model for a Helmholtz resonator liner, J. Sound Vib. 333 (2014) 3536–3549.
[95] R.E. Motsinger, R.E. Kraft, Design and Performance of Duct Acoustic Treatment, Acoustical Society of America, 1995, pp. 165–206.
[96] Jrme Anthoine, Jean-Marie Buchlin, Avraham Hirschberg, Effect of nozzle cavity on resonance in large SRM: theoretical modeling, J. Propuls. Power 18 (2002) 304–311.
[97] S. Gallier, M. Prevost, J. Hijlkema, M. Roumy, Effects of cavity on thrust oscillations in subscale solid rocket motors, in: 45th AIAA/ASME/SAE/ASEE Joint Propulsion Conference & Exhibit, 2009, p. 5253.
[98] Lionel Hirschberg, Thierry Schuller, Jean Collinet, Christophe Schram, Avraham Hirschberg, Analytical model for the prediction of pulsations in a cold-gas scale-model of a Solid Rocket Motor, J. Sound Vib. 419 (2018) 452–468.
[99] L. Hirschberg, S. Hulshoff, J. Collinet, C. Schram, T. Schuller, Vortex nozzle interaction in solid rocket motors: a scaling law for upstream acoustic response, J. Acoust. Soc. Am. 144 (2018) EL46–EL51.
[100] S. Hulshoff, A. Hirschberg, G. Hofmans, Sound production of vortexnozzle interactions, J. Fluid Mech. 439 (2001) 335–352.
[101] J. Avossa, F. Branda, F. Marulo, G. Petrone, S. Guido, G. Tomaiuolo, A. Costantini, Light electrospun polyvinylpyrrolidone blanket for low frequencies sound absorption, Chin. J. Polym. Sci. (English Edition) 36 (2018) 1368–1374.
[102] G. Del Sorbo, G. Truda, A. Bifulco, J. Passaro, G. Petrone, B. Vitolo, G. Ausanio, A. Vergara, F. Marulo, F. Branda, Non monotonous effects of noncovalently functionalized graphene addition on the structure and sound absorption properties of polyvinylpyrrolidone (1300 kda) electrospun mats, Materials 12 (2018).
[103] F. Branda, F. Marulo, S. Guido, G. Petrone, G. Del Sorbo, G. Truda, G. Tomaiuolo, Polyvinylpyrrolidone (Pvp)/Graphene Based Soundproofing Materials through Electrospinning, 2017-January.